# University of Cincinnati

**Date: 10/24/2022**

**I, Tien Dao, hereby submit this original work as part of the requirements for the degree of Master of Science in Electrical Engineering.**

It is entitled:

**Concentrating Solar Thermoelectric Generator Tool**

Student's name: **Tien Dao**

This work and its defense approved by:

**Committee chair: Je-Hyeong Bahk, Ph.D.**

**Committee member: Chong Ahn, Ph.D.**

**Committee member: Marc Cahay, Ph.D.**

**Committee member: Tao Li, Ph.D.**

44138

**Concentrating Solar Thermoelectric Generator Tool**

A thesis submitted to the Graduate School of the University of Cincinnati in partial requirements for the Degree of

Master of Science

in the Department of Electrical Engineering and Computer Science of the College of Engineering and Applied Science

by

**Tien Duy Dao**

Bachelor of Science: Electrical Engineering

University of Cincinnati

May 2020

Committee Chair: Je-Hyeong Bahk, Ph.D.

## Abstract

Solar Thermoelectric (TE) uses thermoelectric modules to absorb radiative energy given off by the sun and convert it into electricity. While its main competition, photovoltaic panels boast an efficiency of around 20%, solar TE panel can only muster around 5-7 % efficiency. This reason along with high material and manufacturing cost has been the cause as to why solar TE has not been extensively explored as an alternative solar energy harvester so far. However, due to the increasing effects of global warming, alternative sources of harnessing energy such as solar TE have been more closely researched. In the past decades, scientists have synthesized new TE materials that have shown great promise in increasing efficiency and power output, surpassing even the properties of Bismuth Telluride-based alloys, which have been widely used for low-temperature TE applications due to having one of the best efficiencies and power output available in the temperature range.

This new materials discovery promises a great new technological innovation for the field of thermoelectric for years to come, but there are not many tools currently available that can simulate the effect of harnessing solar radiation using these materials.

The Concentrating Solar Thermoelectric Generator Tool developed in the work takes advantage of the ever-developing world of thermoelectric materials by inputting users' newly developed or already known thermoelectric properties into the simulation. By using the users' own data, a power output and efficiency can be presented with varying independent variables: the cross-sectional area and thickness of the TE element, solar concentration, and fractional coverage while also taken into consideration the optical parameters and emissivity of the grey surfaces and heat transfer, amongst other data for an ideal optimization of solar TE design.

This tool is intended to bridge the gap between the theoretical and experimental by introducing a way that scientists and researchers can simulate known and theoretical materials. We find that the result adequately depicts power output and efficiency in neat and accurate plots with respect to their independent variable. We describe the methodology for the solar TE design optimization in terms of system efficiency and cost. For the latter, we show that strategically reducing the fractional coverage and thickness of TE elements by similar factors can keep the thermal load matching condition satisfied for system efficiency, while significantly reducing the material cost to ultimately achieve a much-reduced cost per power of $0.07/Watt.

The link for the solar TE tool can be found at: https://nanohub.org/tools/solarte

# Acknowledgement

I want to give a big thank you to my advisor, Dr. Bahk. If it wasn't for Dr. Bahk's Thermoelectric class and our many one-on-one meetings, I truly would not be here today. Throughout the past year, Dr. Bahk has always been there when I needed him; whether it was for asking silly Thermoelectric questions or advice on navigating Graduate school, Dr. Bahk is always one email away. I will always be grateful for his mentorship and guidance as I tackle the challenges of the future.

I would also like to thank my Thermoelectric group members: Yu, Mark, Nilesh, Isaac, Thiraj, Kingsley, Umar, and Ahmad, without them asking questions and critiquing me during our weekly group meeting I would have a difficult time understanding the subjects in this paper. They have truly help me be a better researcher.

Finally, I would like to thank my committee members: Dr. Marc Cahay, Dr. Tao Li, and Dr. Chong Ahn for reviewing and attending my thesis defense.

# Table of Contents

## List of Tables



## List of Figures

## List of Symbols

| Symbol | Description | Unit |
|---|---|---|
| I | Electrical Current | A |
| V | Voltage | V |
| $V_{OC}$ | Open Circuit Voltage | V |
| P | Power/Watts | W |
| $P_{out,max}$ | Max power output | W |
| R | Electrical Resistance | Ω |
| $R_i$ | Internal Resistance | Ω |
| Rc | Contact Resistance | Ω |
| $R_{el}$ | Electrical Resistance | Ω |
| $R_L$ | Load Resistance | Ω |
| $R_{TH}$ | Thermal Resistivity | 1/K |
| $^oC$ | Temperature Celsius | $^oC$ |
| K | Temperature Kelvin | $^oK$ |
| $T_H$ | Temperature on the Hot side | $^oK$ |
| $T_C$ | Temperature on the Cold side | $^oK$ |
| $\Delta T$ | Temperature Difference | $^oK$ |
| S | Seebeck Coefficient | µV/K |
| $\rho$ | Electrical Resistivity | Ω*m |
| σ | Electrical Conductivity | S/m or 1/ $\rho$ |
| $\sigma_{SB}$ | Stefan-Boltzmann Constant | $W/m^2K^4$ or $Btu/h*ft^2R^4$ |

| | | |
|---|---|---|
| C | Solar Concentration Ratio | Suns |
| G | Solar Irradiation | $W/m^2$ |
| $\tau$ | Transmissivity of solar concentrator | - |
| $\alpha$ | Absorptivity of solar absorber | - |
| $\varepsilon$ | Emissivity of TE absorber | - |
| $\kappa$ | Thermal Conductivity | W/m*K |
| $A_p$ | Leg Area, p-type | $mm^2$ |
| $A_n$ | Leg Area, n-type | $mm^2$ |
| $L_p$ | Leg Thickness, p-type | mm |
| $L_n$ | Leg Thickness, n-type | mm |
| $\eta$ | Efficiency | % |
| $\eta_{TE}$ | Thermoelectric Efficiency | % |
| $Q_H$ | Heat Input | W |
| $Q_{Peltier}$ | Peltier Heat | W |
| $Q_{Comd}$ | Heat of conduction | W |
| $Q_{Joule}$ | Joule Heating | W |
| $Q_{in,TE}$ | Heat input to the TE | W |
| $Q_{in,sys}$ | Heat input to the system | W |
| $Q_{in,total}$ | Total heat input | W |
| $Q_{conv,out}$ | Air convection heat loss | W |
| h | Heat Transfer Coefficient | $W/m^2K$ |

| | | |
|---|---|---|
| $\psi_C$ | Heat Transfer Coefficient Cold-Side | W/m$^2$K |
| $\psi_H$ | Heat Transfer Coefficient Hot-Side | W/m$^2$K |
| F | Fill Factor | - |
| $N_{TE}$ | TE leg pairs | - |
| N | Number of Segments | - |

# 1. Introduction

## 1.1 Solar Technologies

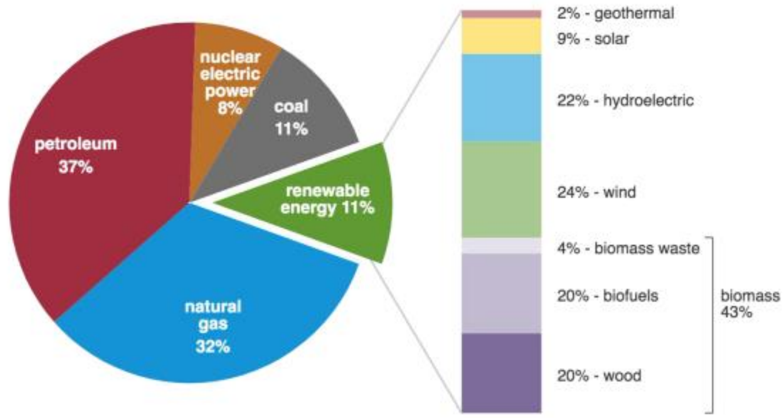


*Figure 1: U.S. Energy Consumption 2019 [1]*

According to the U.S. Energy Information Administration data, in 2019, 11% of energy the U.S. consumes come from renewable energy such as wind and solar, while the majority of our energy need comes from nonrenewable energy such as coal and natural gas. Nonrenewable energy, by definition, will eventually be depleted [2]; due to this as well as the huge problem of contributing to the effect of global warming, the world needs to make an urgent priority towards the research and development of other forms of renewable energy. One of the solutions is the harvesting of solar energy.

Every hour, the Earth is bombarded with 173,000 TW of solar energy by sunlight, this is more than the total energy the world consumes in a single year [3]. However, only 9% of renewable energy is solar energy, the majority of which is collected by conventional photovoltaic (PV) solar panels.

PV panels works by using N and P type Silicon joined together to form a p-n junction and create an electric field. As the p-n junction absorbs sunlight, the electrons in the N type moved to the P type while the holes in the P type moved to the N type, creating an electric current [4].

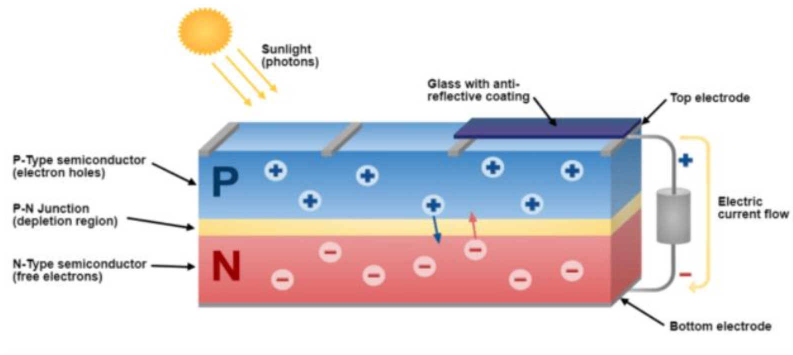


*Figure 2: Photovoltaic Effect [5]*

Solar TE, which are not yet offered for public purchase, uses the heat from sunlight to generate electricity and is another possible solution to harness this free energy. Solar TE uses the temperature difference between the top and bottom Thermoelectric Generator (TEG) plate to create a current. A schematic of a TEG is shown in the Figure 3 below.

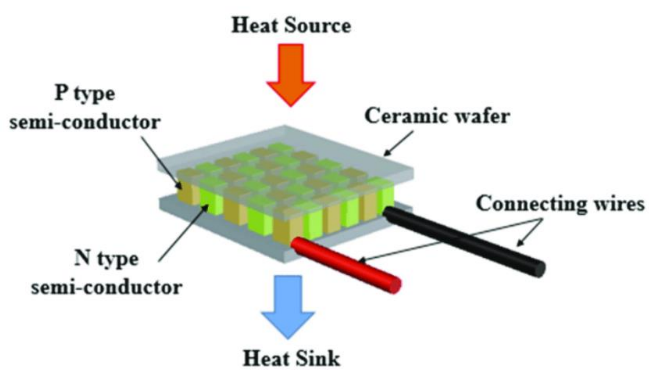


*Figure 3: TEG Schematic [6]*

Examples of TEG includes catalytic converters found in vehicle that are used to convert waste and toxic heat into energy as well as Radioisotope Thermoelectric Generator (RTG) used in the early 1960s by NASA's spacecrafts: Voyager I and Voyager II.

While the power generation in Solar TEG are not as substantial as compared to conventional photovoltaic cells, their reliability and low form factor are a few advantages that many researchers point to as evidence for further research in this field as well as substantial material development in past decades that points to continued improvement in power and efficiency that could someday rival PV solar panels.

This thesis introduces a tool that simulate the output of a Solar Thermoelectric (solar TE) generator by converting a heat source in the form of sunlight into electricity utilizing the Seebeck effect and Peltier effect while also accounting for basic heat transfer mechanisms such as radiation, convection, and conduction.

## 1.2 Motivation

While much research and studies have been put into understand how better harness the power of the sun through the use of PV solar panels, solar TE have never received the same treatment due to its lack of efficiency and high cost compared to conventional PV.

However, recent advances in thermoelectric material have given hope to bridge the efficiency gap between solarte and PV with materials such as hole-doped $Na_{0.03}Sn_{0.965}Se$, which have been shown in lab to output a ZT, the figure of merit that determines the maximum energy conversion at a given temperature, of 3.1 at 783$^{o}$K [7] and p-type PbTe have been shown to have a ZT of around 2.0 [8] compared to Bismuth Telluride's ZT of around 1 which have been used since the early 1960s.

The solar TE simulation tool presented in this thesis offer scientists a quick and easy way to test out newly developed and theoretical temperature dependent TE materials for better understanding and for comparison against conventional PV solar panels.

# 2. Background

## 2.1 Seebeck Effect

The Seebeck effect, which maybe refer to as Thermoelectric effect is described as the conversion of temperature difference into electricity and can be best described by

$$S = \frac{V}{\Delta T} = \frac{E}{\nabla \mathrm{T}} \ (1)$$

Where S is the Seebeck coefficient, which is the measure of a material's ability to transform heat into electricity, V is the electrical voltage, and $\Delta T$ is the temperature difference between the hot side and cold side of a thermocouple and ∇T is the temperature gradient and is described as

$$\nabla \mathrm{T} = \frac{\Delta \mathrm{T}}{L} \ (2)$$

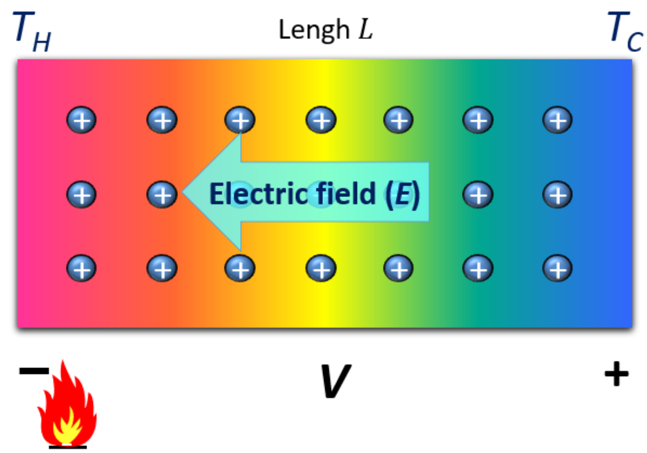


*Figure 4: Seebeck Effect on Module [9]*

When heat is applied, for P-type materials, holes accumulate at the cold side while electrons migrate to the hot side, creating an electric field and voltage is generated from the cold side to the hot side.

### 2.2 Peltier Effect

Peltier effect occurs when a current is passed through two dissimilar Seebeck coefficients. As a result, heat is generated on one side while a cooling effect occurs on the other side, an example is shown in the figure below.

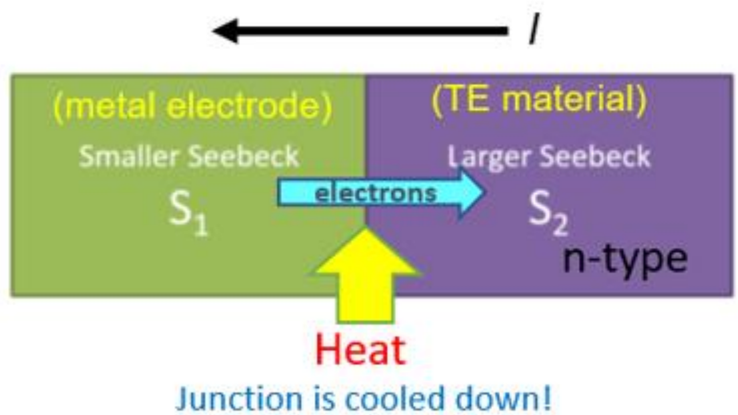


$$\Pi_1 = S_1 \cdot T \qquad \Pi_2 = S_2 \cdot T$$

$$(\Pi_2 - \Pi_1)I = (S_2 - S_1) \cdot T \cdot I$$

*Figure 5: Peltier Effect Example [9]*

As current is passing from a lower Seebeck to a higher Seebeck material, more energy in the form of heat needs to be absorbed from the environment thereby cooling down the environment while compensating for the potential energy difference.

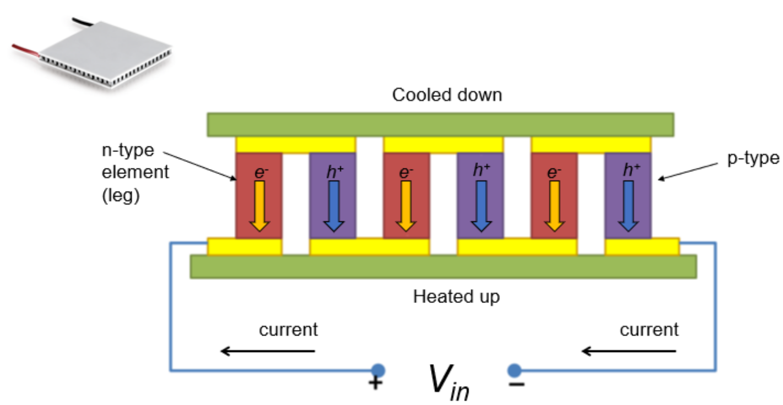


*Figure 6: Peltier Module [9]*

In a single leg TEG module, the voltage that are generated from an individual TE element are often very small to do any useful work. To solve that problem, the TE elements are often connected (in a $\pi$-shaped) to each other with alternating n-type and p-type TE material in a series with heat absorbing material on both sides to maximize efficiency.

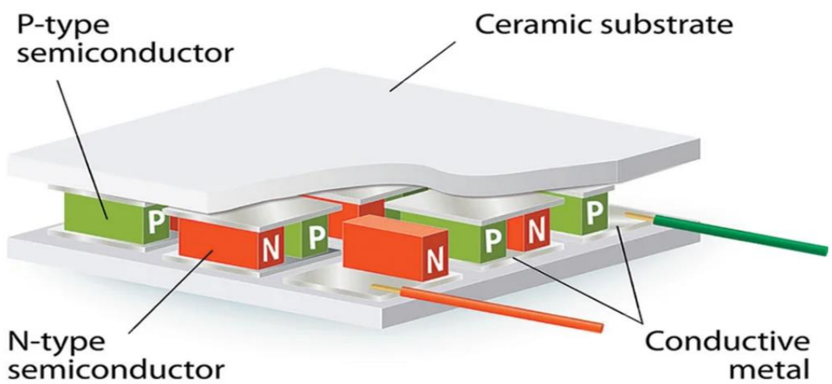


*Figure 7: TEG Module in Series (π-module) [10]*

## 2.3 Thermoelectric

### 2.3.1 Single Leg Thermoelectric Generator

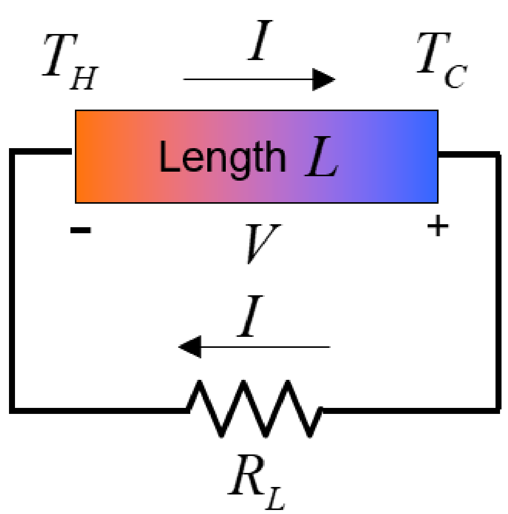


*Figure 8: Single-Leg TEG with Connected Load [9]*

In a single-leg TEG with a load connected, the open circuit and load voltage is calculated as

$$V_{OC} = S(T_H - T_C) \ (3)$$

$$V_L = V_{OC}\frac{R_L}{R_L+R_i} \ (4)$$

with $R_i$ being the internal resistance of the TE material and circuit.

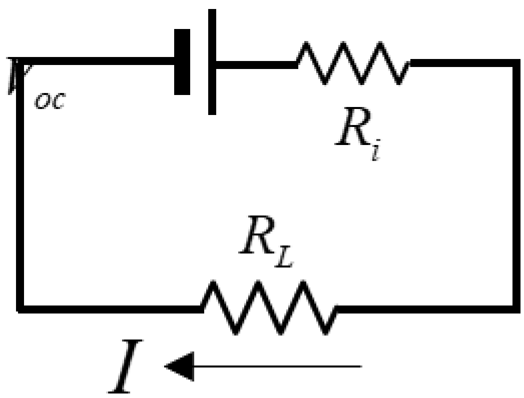


*Figure 9: Single-Leg Equivalent Electrical Circuit [9]*

The current is calculated as

$$I = \frac{V_{OC}}{R_L+R_i} \ (5)$$

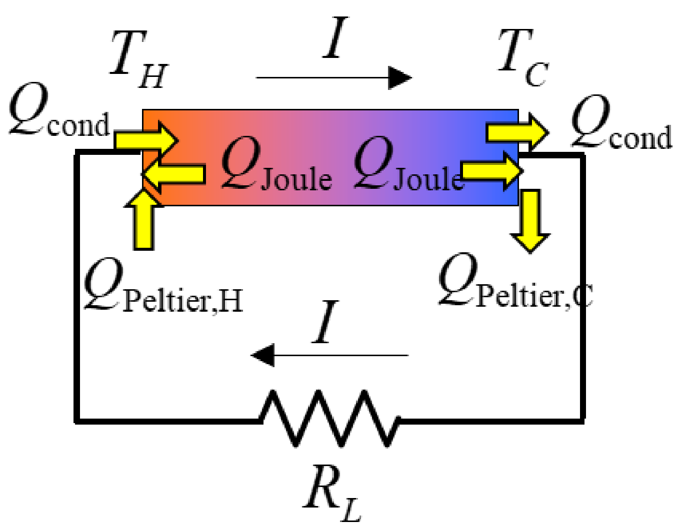


*Figure 10: Single-leg Thermal Analysis [9]*

Calculating Thermal Analysis with

$$Q_H = Q_{Peltier,H} - Q_{Joule} - Q_{Cond} \ (6)$$

$$Q_C = Q_{Peltier,C} + Q_{Joule} + Q_{Cond} \ (7)$$

With

$$Q_{Peltier,H} = ST_H I \ (8)$$

$$Q_{Peltier,C} = ST_C I \ (9)$$

$$Q_{Joule} = \frac{1}{2} I^2 * R \ (10)$$

$$Q_{Cond} = K \, \Delta\mathrm{T} \ (11)$$

Where K is the thermal conductance that is a temperature dependent intrinsic value of each material.

Efficiency is the measure of how competent a system is able to do its job with as little input as possible while maximizing the output. In Thermoelectric, efficiency is the ratio of how much power is generated to the rate of heat input. For single leg TEG, their values can be calculated as

$$\eta = \frac{W}{Q_H} = \frac{P_{Out}}{Q_H} \ (12)$$

where

$$W = I^2 * R_L \ (13)$$

which can also be written as

$$P_{out} = \frac{R_L * S^2 * (\Delta T)^2}{(R_L + R)^2} \quad (14)$$

To maximize power output and efficiency of single leg TEG, $P_{out}$ and $\eta$ can be differentiated to get

$$P_{Out,max} = \frac{S^2 * (\Delta T)^2}{4 * R} \quad (15)$$

with load matching, when $R = R_L$

and

$$ZT = \frac{S^2 * \sigma}{\kappa} T \quad (16)$$

ZT is the thermoelectric figure of merit. It is used in the world of thermoelectric to determine the maximum efficiency of a TE material.

### 2.3.2 Coupled-Leg Thermoelectric Generator

Coupled-leg TEG applied the same concept found in single-leg TEG and expands on to include both n-type and p-type TE material.

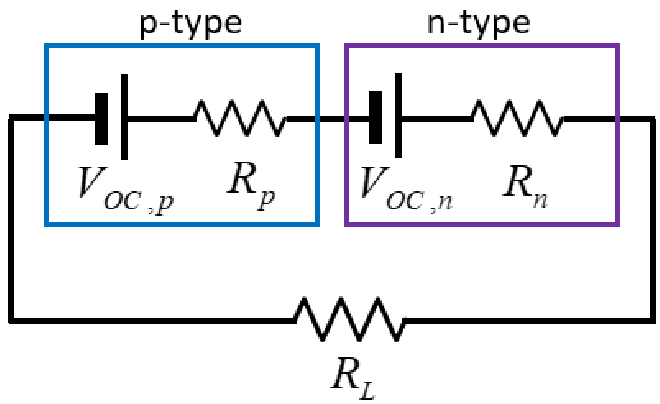


*Figure 11: Coupled-Leg TE Circuit [9]*

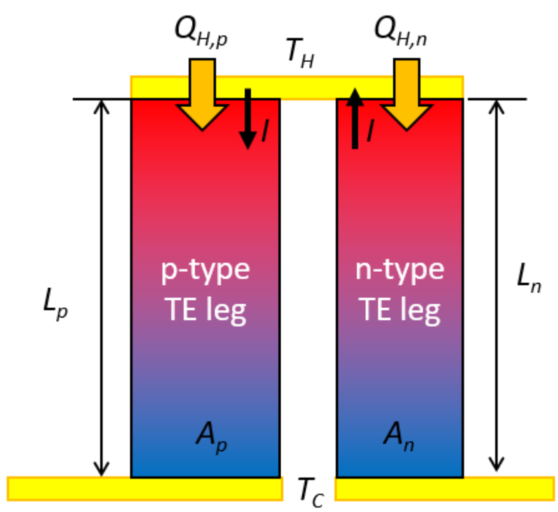


*Figure 12: Coupled-Leg TEG [9]*

The heat input can be calculated as

$$Q_H = Q_{H,p} + Q_{H,n} = ST_H I - \frac{1}{2} * I^2 R + K\Delta\mathrm{T} \ (17)$$

where the heat input on the p-type is

$$Q_{H,p} = S_p T_H I - \frac{1}{2} * I^2 R_p + K_p \Delta\mathrm{T} \ (18)$$

and the heat input on the n-type side is

$$Q_{H,n} = -S_n T_H I - \frac{1}{2} * I^2 R_n + K_n \Delta T \ (19)$$

where

$$S = S_p + S_n \ (20)$$

$$R = R_p + R_n \ (21)$$

$$K = K_p + K_n \ (22)$$

and like single-leg, power output can be similarly calculated with equation 14 with R and S values calculated in equation 20, 21, and 22.

Coupled leg TEG efficiency is similarly calculated using equations 12, 14, and 15.

## 2.4 Heat Transfer

Heat transfer is the flow of heat from hot objects to cold object when there is a temperature difference between the two [11]. It is extensively used when converting energy from the sun to the energy received by the TE module. Heat transfer occurs in three ways: Conduction, Convection, and Radiation. All three forms are present in the simulation and will be explained in the following sections.

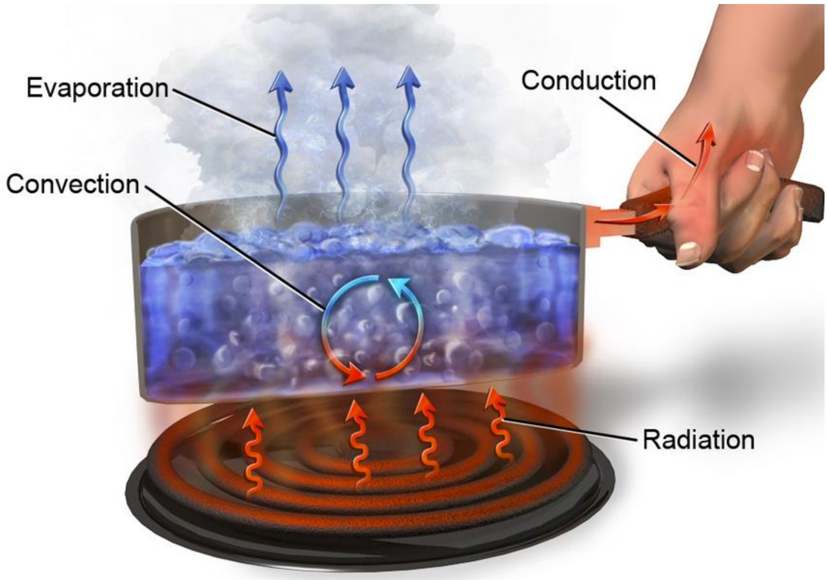


*Figure 13: Heat Transfer Mechanism [12]*

### 2.4.1 Conduction

Conduction is the physical transfer of heat of atoms through direct contact with neighboring atoms and only occur between solid materials [12]. When exposed to energy (often in the form of increased temperature) the atoms within the particles become excited and starts vibrating, creating kinetic energy. This energy, in turns causes the surrounding particles to heat up.

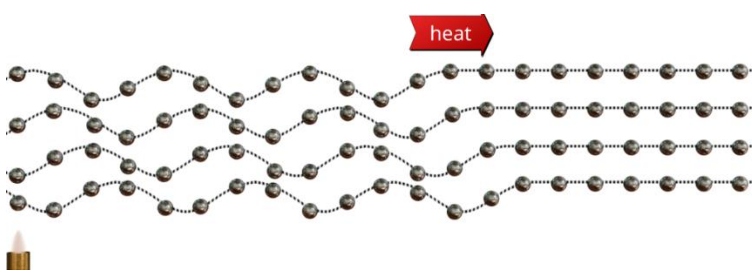


*Figure 14: Conduction Example [9]*

### 2.4.2 Convection

Convection occurs in liquid and gas phases. It describes the motion of fluid when energy is added to the system. As energy is added, the hot fluid will rise to the top while the cold fluid sinks to the bottom. The cycle continues until the energy added is depleted [9][13]

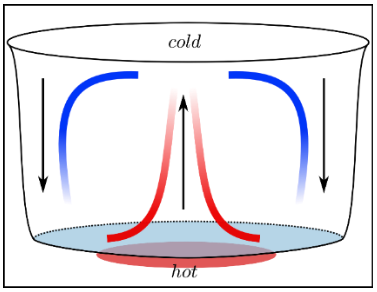


*Figure 15: Convection Example [9]*

Two forms of convection are studied: Natural and Forced Convection. Natural convection occurs when there are no external forces acting on the fluid and when there is difference in temperature. An example of which can be found when boiling water. As the temperature increases at the bottom of the pot, the hotter part of the fluid becomes less dense and rises due to buoyancy while the cooler and denser fluid to descend, thereby, creating a cycle [9] [13].

Forced convection occurs when an external force is used to create the convection, such as a pump or a fan. One example of this is an air conditioning unit found inside a home. The data for convective heat transfer coefficient can be found in Table 1 below.

| Flow type | (W/m² K) |
|---|---|
| Forced convection; low speed flow of air over a surface | 10 |
| Forced convection; moderate speed flow of air over a surface | 100 |
| Forced convection; moderate speed cross- flow of air over a cylinder | 200 |
| Forced convection; moderate flow of water in a pipe | 3000 |
| Forced Convection; molten metals | 2000 to 45000 |
| Forced convection; boiling water in a pipe | 50,000 |
| Forced Convection - water and liquids | 50 to 10000 |
| Free Convection - gases and dry vapors | 5 to 37 |
| Free Convection - water and liquids | 50 to 3000 |
| Air | 10 to 100 |
| Free convection; vertical plate in air with 30°C temperature difference | 5 |
| Boiling Water | 3.000 to 100.000 |
| Water fowing in tubes | 500 to 1200 |
| Condensing Water Vapor | 5.0 - 100.0 |
| Water in free convection | 100 to 1200 |
| Oil in free convection | 50 to 350 |
| Gas flow on tubes and between tubes | 10 to 350 |

*Table 1: Types of Convective Heat Transfer Coefficient [14]*

### 2.4.3 Radiation

Radiation is the heat transfer between two objects at distance without a medium in between. Radiation heat transfer includes all spectrums in the electromagnetic spectrum such as ultraviolet, infrared, X-ray and so on as long as there is a temperature difference between the objects 9]. Thermal radiation is expressed by the Stefan-Boltzmann Law of Radiation as

$$Q_r = A_1 \varepsilon_1 \sigma_{SB} (T_1^4 - T_2^4) \; (23) \; [9]$$

where $A_1$ is the surface area of the object, $\varepsilon_1$ is defined as the emissivity which is the energy absorption rate with black being $\varepsilon = 1$ and $\varepsilon = 0$ for a perfectly reflecting object, $\sigma_{SB}$ is the Boltzmann constant with the value of $5.67 \times 10^{-8}$ W/m$^2$K$^4$, $T_1$ and $T_2$ are the temperature of the receiving or emitting object. An example of thermal radiation can be found in Figure 13 above.

Examples of radiation are nuclear and solar energy radiation, both of which are sources of renewable energy.

# 3. Literature Review

## 3.1 Solar TEG Tool – Segment TEG

Madkhali and Lee proposed a tool that could achieve an efficiency of 21.6% and a respectable power output of 5.7 W for a 9 $cm^2$ absorber area and a solar concentration of 30 suns [15]. The simulation operates in ANSYS and is consists of the materials shown below.

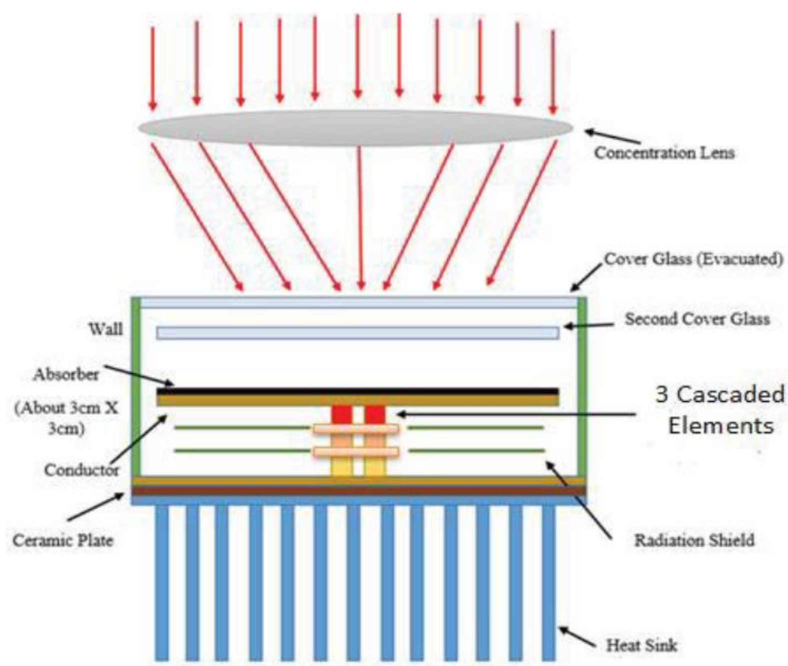


*Figure 16: TE Design [15]*

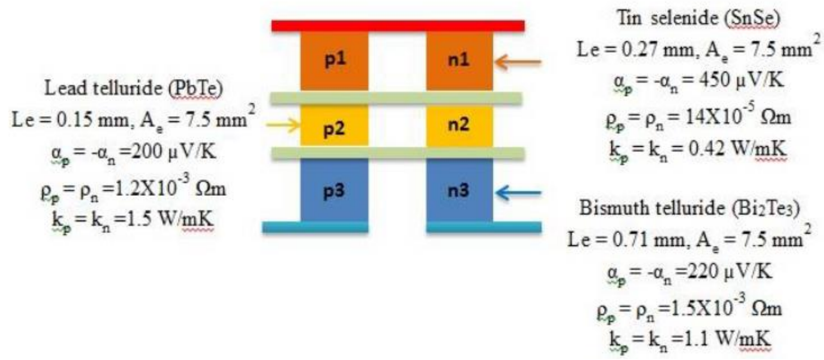


*Figure 17: TE Segment prototype [15]*

This tool tried to take advantage of the fact that each temperature dependent TE material is the most efficient at certain temperature range i.e., best ZT. In the simulation, the concentration focused the sun light on 2 glass panes by radiation and hits the solar absorber where it is then by conduction, transfer to the top TE element, Tin Selenide (SnSe) at around 1000$^{o}$ K, which have been shown to have a ZT of 2.6 at around 900 – 1000$^{o}$K for N and P-type, before moving down to PbTe and BiTe, where each element is efficient at converting heat into electricity and their respective temperature range.

While this is a promising approach to modeling solar TE, scale up production will be a challenge for scientists and engineers due to the manufacturing cost that must be taken into consideration. The 6 different TE materials, which changes price based on market value everyday as well as the cost for the radiation shield and 3 pieces of glass will significantly drive up the $/W for the average consumer.

Also, this simulation does not incorporate temperature dependent TE material. While each element is assigned their own TE properties based on a particular temperature that the element will exhibit, as heat moves down the TE elements, temperature drops but the original TE properties are still being used for calculation. Incorporating temperature dependent TE properties will give the simulation more accuracy in calculating power output and efficiency.

### 3.2 Solar TEG Tool - Lateral Solar Micro-TEGs

Unlike the conventional vertically nanostructure oriented, Leon et al in 2012 proposed a simulation of solar TEG that utilize a lateral structure using COMSOL [16]. This design still takes advantage of the concentrating lens use for focusing the heat influx as well as TE elements. In Figure 18a, sunlight is focus on the lens and passed onto the central area of the TEG called the membrane. As the heat radiates out towards the outer perimeter, the temperature closer to the center will be higher than the ones in the outer perimeter, creating a temperature difference, shown in Figure 18b. With a concentrating factor of 900, a max Carnot efficiency of 30% is possible, rivalling even those of solar cells.

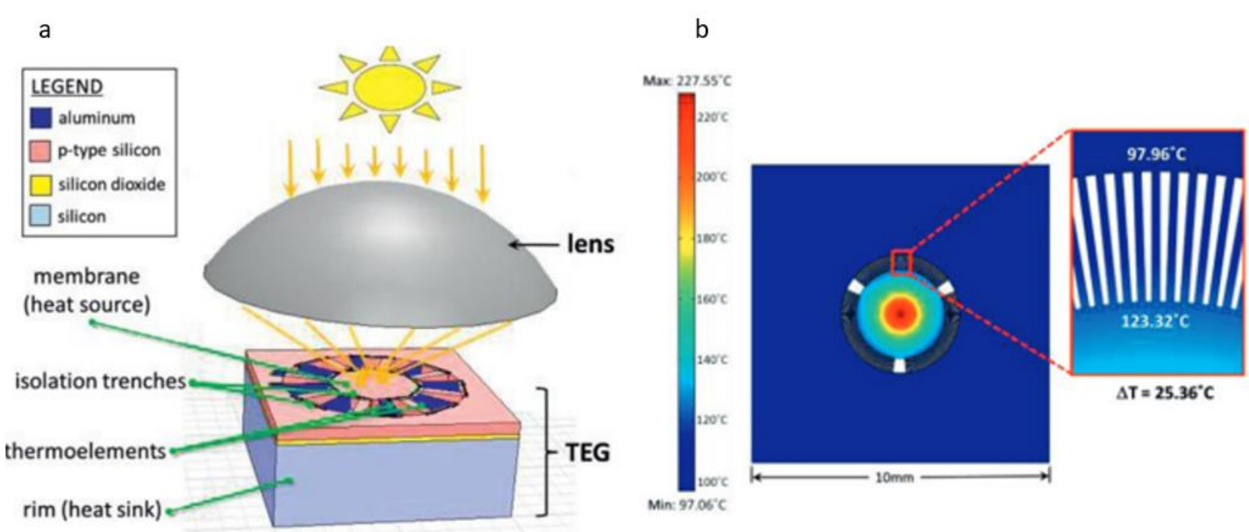


*Figure 18a) Concentrating Solar TEG Proposal b) Heat Transfer Simulation [16]*

This approach proposed a new and innovate way harness solar energy but requires more data for evidence of research such as simulating with different TE materials.

# 4. Tool Design

## 4.1 Theory

The radiative input is the amount of energy absorb from the sun and is given by

$$Q\text{rad, in} = GC\tau\alpha A_{\text{total}} (24)$$

where G is the amount of solar irradiation falling upon the TE absorber area expressed in W/m$^2$, C is the solar concentration which is the ratio of solar concentrator area to the TE absorber area which is expressed as suns, $\tau$ is the transmissivity of the concentrator which is the percentage of heat the concentrator passed through, $\alpha$ is the absorptivity of the solar absorber which is the percentage of solar irradiation the TE surface absorbs, and A is the area of the TE absorber plate [17].

The radiative output is the heat loss that occurs when there is a radiation exchange between the plate surface and its surroundings given by the Stefan-Boltzmann Law of Radiation

$$Q_{\text{rad,out}} = \varepsilon\sigma_{SB} A_{\text{total}} \left(T_{\text{top}}^4 - T_{\text{amb}}^4\right) \text{ (25)}$$

with $\varepsilon$ as the emissivity which is the ratio of the energy being dissipated from the material's surface compared to that of a perfect emitter [18].

Convection heat loss also needs to be factored with $h_{\text{conv}}$ as a constant.

$$Q_{\text{conv,out}} = h_{\text{conv}} A_{\text{total}} (T_{\text{top}} - T_{\text{amb}}) \text{ (26) [14] [17]}$$

Total heat input entering the TE element is calculated as

$$Q_{\text{in,total}} = Q_{\text{rad,in}} - Q_{\text{rad,out}} - Q_{\text{conv,out}} \quad (27)$$

## 4.2 Finite Element Method

In this temperature dependent TE tool, the Finite Element Method is used. In this method, n and p-type TE element is divided into N equal segments with $S_i$, $\sigma_i$, and $\kappa_i$ being TE properties are assigned at the i$^{\text{th}}$ segment depending on its temperature shown in Figure 19a.

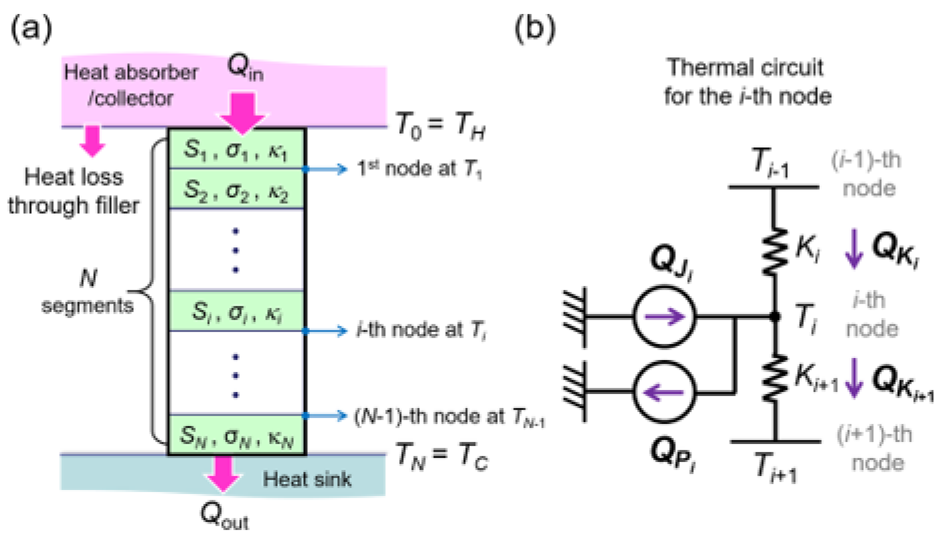


*Figure 19 a) Finite Element Method b) Equivalent Thermal Circuit [17]*

This process works by assigning temperature at each node. At node i, an initial guess for the temperature is used with appropriate TE properties based on node i-1, the heat balance equations are then used to update the temperature profile. Based on the updated temperature profile, temperature at node i+1 is then estimated. The process is repeated until all nodes and heat equations are calculated. This process is applied to both n and p-type TE material used in the simulation. Once all temperature profiles are determined, $T_i$ from N and P type are then compared until all temperature values converges within an acceptable tolerance.

The heat equations: Joule heat, Peltier heat, and conduction heat, traveling across each segment in Figure 19b is defined respectively in equations below with $R_i = L_{TE}/(\sigma_i A_{TE} N)$ and $K_i = (\kappa_i A_{TE} N)/L_{TE}$ with $A_{TE}$ being the cross sectional area of the TE element.

$$Q_{J_i} = \frac{1}{2} I^2 R_i + \frac{1}{2} I^2 R_{i+1} \quad (28)$$

$$Q_{P_i} = (S_{i+1} - S_i) T_i I \quad (29)$$

$$Q_{K_i} = (T_{i-1} - T_i) K_i \quad (30)$$

At the i-th node, the heat balance equation is

$$Q_{J_i} - Q_{P_i} + Q_{K_i} - Q_{K_{i+1}} = 0 \; (31)$$

Current is solved using standard Ohm's Law

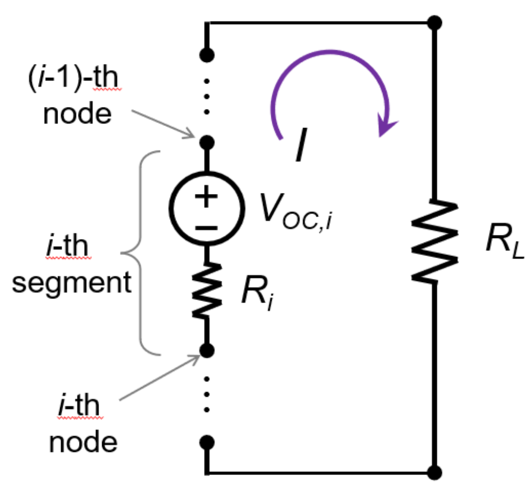


*Figure 20: Electrical Circuit [9]*

Internal resistance in series is added with contact resistance along with internal electrical resistance gives the total internal resistance as

$$R_{\mathrm{int}} = \sum(\sum_i R_i + 2R_c + 2R_{\mathrm{el}}) \ (32)$$

The open circuit voltage for each segment is calculated based on the Seebeck effect as

$$V_{\mathrm{OC}_i} = S_i(T_i - T_{i-1}) \ (33)$$

Total open circuit voltage is obtained by adding all $V_{\mathrm{OC}_i}$ of the segments of the TE elements

$$V_{\mathrm{OC}} = \sum \sum_i V_{\mathrm{OC},i} \ (34)$$

Using Ohm's Law to calculate resulted current

$$I = \frac{V_{\mathrm{OC}}}{R_{\mathrm{int}} + R_L} \ (35)$$

At i = 0, with current at 0 and $T_0 = T_H$

$$Q_{J_0} = \frac{1}{2} I^2 R_1 (36)$$

$$Q_{P_0} = S_1 T_0 I \ (37)$$

The Fill Factor, F, is the fractional coverage area by the TE elements over the entire module area is described as

$$F = \frac{N_{\mathrm{TE,pair}}(A_n + A_p)}{A_{\mathrm{total}}} \ (38)$$

here $N_{\mathrm{TE,pair}}$ is the number of n and p-type TE element pairs, $A_n$ and $A_p$ is the cross-sectional area of the element, and $A_{\mathrm{Total}}$ is the surface area of the TE element.

$$Q_{K_1} = (T_0 - T_1)K_1 \text{ (39)}$$

$$Q_{K_0} = \frac{1}{F}A_{TE}\psi_h\left(T_{\text{top}} - T_0\right) - \frac{(1-F)}{F}\frac{A_{TE}}{L_{TE}}k_{\text{filler}}(T_0 - T_N) \text{ (40)}$$

$Q_{K_0}$ is calculated with the heat transfer coefficient on the top plate and subtracting the heat loss due to the $k_{\text{filler}}$ which is the thermal conductivity of the gap between TE elements (usually air = 0.04 W/mK) to get the total heat input.

On the bottom side (cold side), similar equations are being calculated. Equations 20 and 21, does not have current flow at the very bottom, therefore

$$Q_{J_N} = \frac{1}{2}I^2R_N(41)$$

$$Q_{P_N} = S_NT_NI(42)$$

with $T_N = T_C$.

$Q_{K_{N+1}}$ is determined by the heat transfer coefficient at the cold plate

$$Q_{K_N} = (T_{N-1} - T_N)K_N \text{ (43)}$$

$$Q_{K_{N+1}} = A_{TE}\psi_C(T_N - T_{\text{bot}}) \text{ (44)}$$

Lateral heat flow is added to the $Q_{\text{in},n}$ equation because n and p-type materials' temperature profiles are obtained separately and have different TE properties, therefore the top side temperature of p-type is different from the top side of n-type. However, the hot plate is made of thermally conducting material for efficient heat transfer so the temperature on the top side quickly stabilizes. Lateral flow is added to compensate for the uneven temperature distribution, thus for n-type element

$$Q_{\text{in},n} = Q_{K_0,n} = \frac{1}{F} A_{\text{n}} \psi_h \left(T_{\text{top}} - T_0\right) - \frac{(1-F)}{F} \frac{A_{\text{n}}}{L_{\text{n}}} k_{\text{filler}} (T_0 - T_N) - Q_{\text{lateral}} \quad (45)$$

and p-type element, by energy conservation

$$Q_{\text{in},p} = Q_{K_0,p} = \frac{1}{F} A_{\text{p}} \psi_h \left(T_{\text{top}} - T_0\right) - \frac{(1-F)}{F} \frac{A_{\text{p}}}{L_{\text{p}}} k_{\text{filler}} (T_0 - T_N) + Q_{\text{lateral}} \quad (46)$$

Common equations below are then calculated for plotting.

$$V_{\text{out}} = I R_L \quad (47)$$

$$P_{\text{out}} = I V_{\text{out}} \quad (48)$$

$$Q_{\text{in,TE}} = N_{\text{TE,pair}} (Q_{\text{in},n} + Q_{\text{in},p}) \quad (49)$$

$$\eta_{TE} = \frac{P_{\text{out}}}{Q_{\text{in,TE}}} \quad (50)$$

$$\eta = \frac{P_{\text{out}}}{Q_{\text{in,system}}} \quad (51)$$

## 4.3 Tool Overview

The tool proposed in this thesis is divided into 4 parts: Concentrator, Solar Absorber, TE Elements, and Heat Sink.

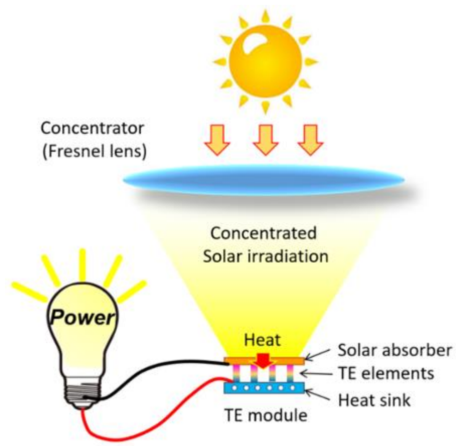


*Figure 21: SolarTE Model [9]*

### 4.3.1 Concentrator

A Fresnel lens is used as the concentrator. A Fresnel lens is different from the conventional lens in that it is a flat optical component where the bulk of the material is removed. The surface is made mostly of concentric grooves and each groove acts like an individual prism to focus the light. [19]. The Fresnel lens determines the number of solar concentrations (suns) absorb into the absorber area and the transmissivity.

A comparison is shown in Figure 22 below showing that the Fresnel lens is thinner than the conventional lens and therefore require less material, however, some disadvantages that needs to be considered includes higher manufacturing cost and edge imperfection which can cause the rays to be unreliable for focusing [19].

A top view is shown in Figure 23.

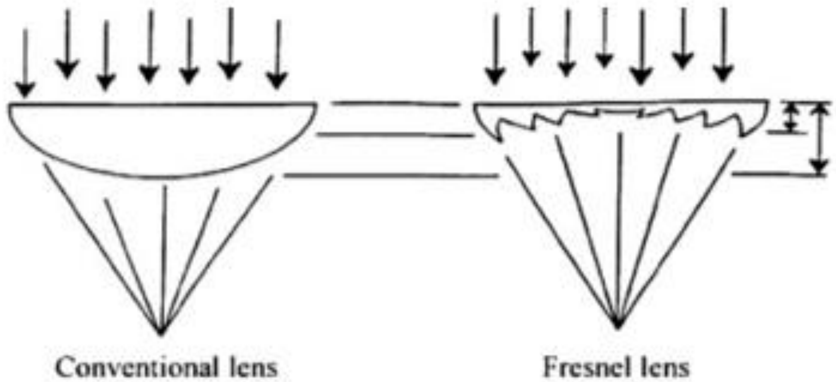


*Figure 22: Fresnel vs. Conventional Lens [20]*

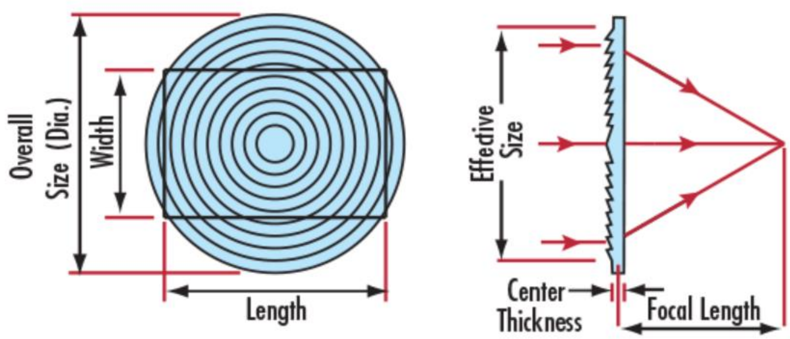


*Figure 23: Fresnel Lens Top and Side View [21]*

### 4.3.2 Solar Absorber

Solar Absorber are materials that are used for absorbing light while keeping it from re-emission as much as possible. The default values for absorbance of 0.9 and emissivity of 0.15 are based on a W/Ni-filled $Al_2O_3$ solar absorber material [22] which uses a method called Double-Cermet Layer to polish a stainless-steel substrate and depositing Nickel and Tungsten on top of an IR coating. An additional layer of $Al_2O_3$ is then applied which is thermally stable in a vacuum at

600° C [22] [23]. Figure 24 demonstrates the layer described with Cermet 1 and 2 as Nickel and Tungsten respectively and $Al_2O_3$ is the antireflection coating (ARC 1). ARC 2 is not used because another layer of coating is not needed.

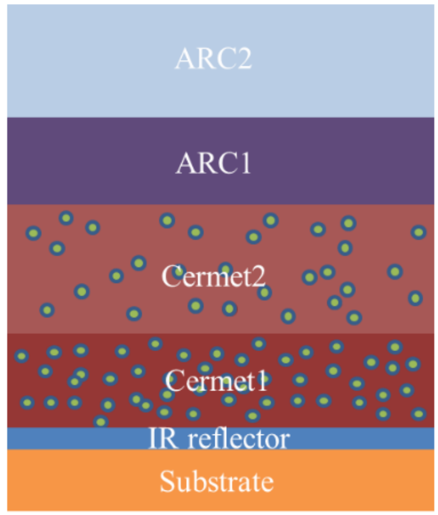


*Figure 24: Double-Cermet Layer [23]*

### 4.1.3 TE Elements

Constant temperature independent as well as temperature dependent TE properties of n-type and p-type materials can be input. The materials are shaped in a "π" configuration as shown in Figure 25. In this "π" configuration, n and p-type are connected electrically in series with metallic layers on top and bottom on each leg, a solder substrate is then placed on top and bottom of each TE stack for proper heat transfer [24]. This is the conventional method for stacking TE materials and the least expensive method for fabrication.

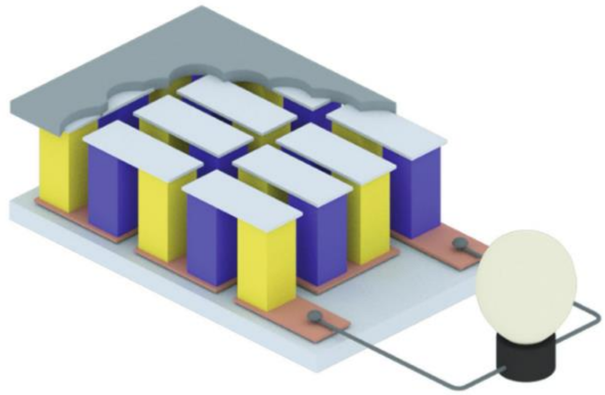

*Figure 25: A "π" TEG Configuration [24]*

### 4.1.4 Heat Sink

A water-cooling heat sink is placed at the bottom on the module for efficient heat removal and to keep the temperature between the hot side and the cold side of the TE module sufficiently high for a high efficiency. A high efficiency water-cooled heat sink can reach the heat transfer coefficient of 4000 $W/m^2K$ but a conservative default value of 3000 $W/m^2K$ is chosen. Research have shown that power output increases and becomes flattens when the heat transfer coefficient on the cold side reaches 4000 $W/m^2K$ and low output is shown at values below 3000 $W/m^2K$ due to the lack of heat dissipation, causing the cold side to increase in temperature, limiting the temperature difference seen in Figure 26 below. Users must also keep in mind that increasing the heat transfer coefficient also works adversely in driving down the system efficiency [17].

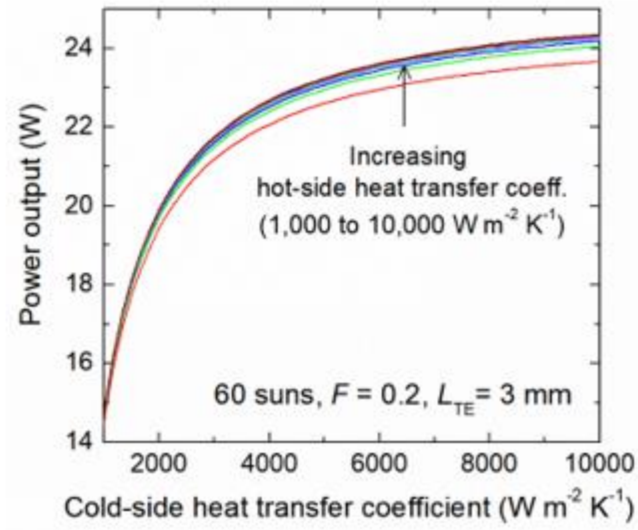


*Figure 26: Cold Side Heat Transfer Coefficient vs. Power Output [17]*

## 4.2 MATLAB

Research data on TE and radiative heat recovery from [9][17] were compile into MATLAB files for development and testing. Afterward, the results were compared with the data collected in laboratory. The data collected in the laboratory were found to be acceptable compared to the simulated result. The algorithm and core code were modified to work as a tool on nanoHUB prior to the author's participation in the research project but the author was able to expand greatly on the capabilities of the tool such as creating a brand-new Summary table and algorithm for calculating and plotting of ZT values.

## 4.3: Design Input Layout

The developed tool performs simulations of harvesting of solar energy using thermoelectric material. In Figure 27, users can choose from 1 of 4 relevant independent variables (cross sectional area of TE material, leg length of TE Material, solar concentrations, and fill factor) to run as simulation. Users can choose to simulate with constant TE properties (Seebeck coefficient, Electrical conductivity, and Thermal conductivity), simulate with their own temperature dependent thermoelectric n and p-type data, or select from an already uploaded list of well-known TE materials such as BiTe and PbTe to name a few. Users can also input various values that affect the outputs such as solar concentrations and length properties of the TE, to name a few, by selecting the appropriate blue dots next to the name.

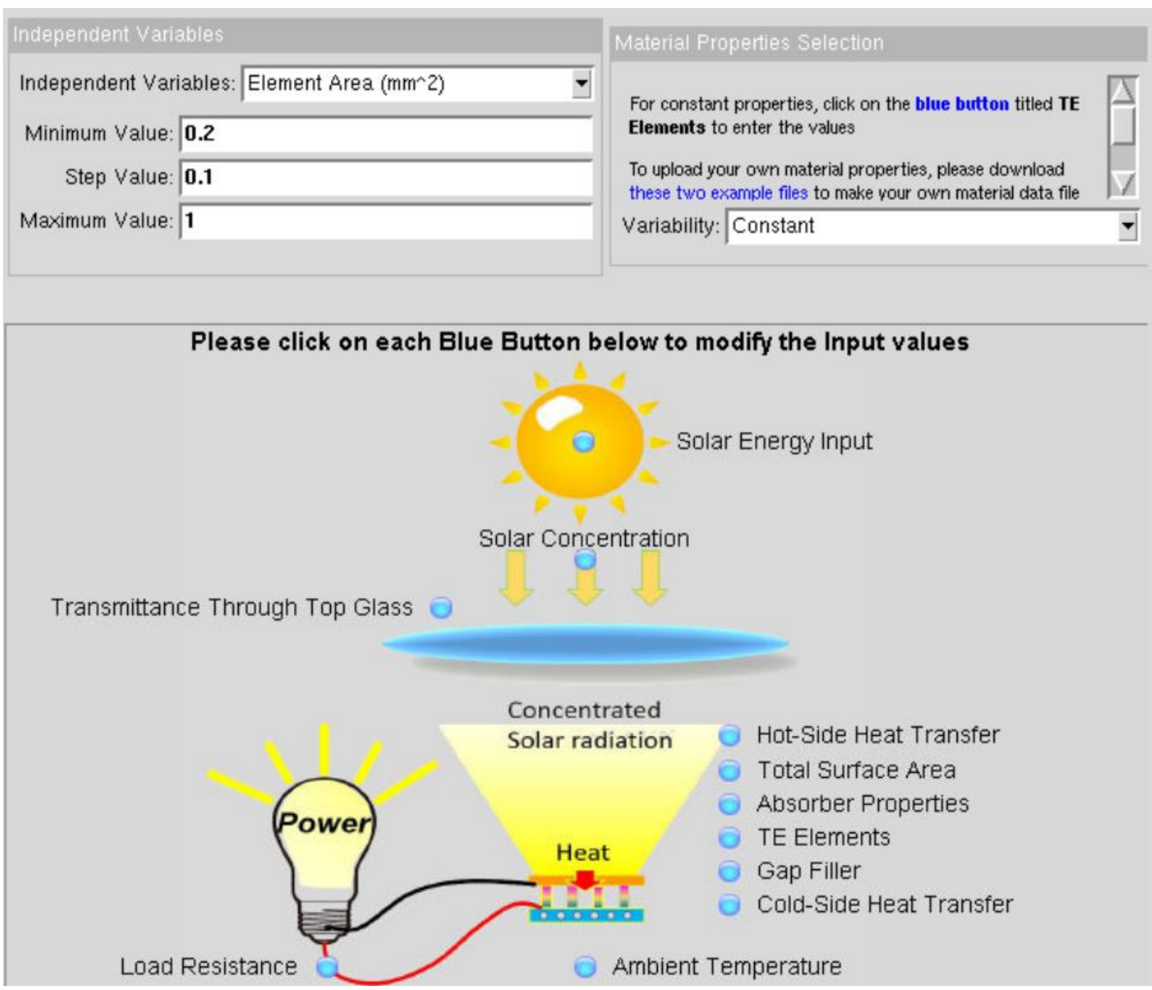


*Figure 27: Simulation Layout*

## 4.4: Design Output Layout

All relevant outputs such as Power Output and Thermoelectric Efficiency can be selected and view on a plot with respect to the independent variable. A drop-down list displays what output will be plotted in the figure below.

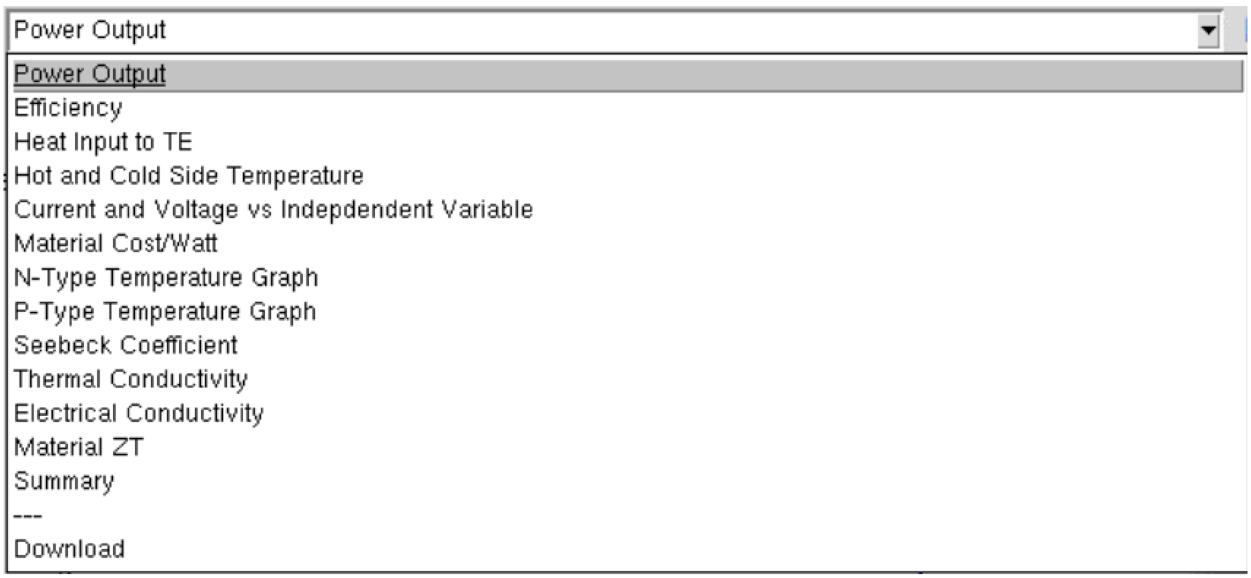


*Figure 28: Output List*

An example plot is also shown in Figure 29 to display what the Power Output looks like.

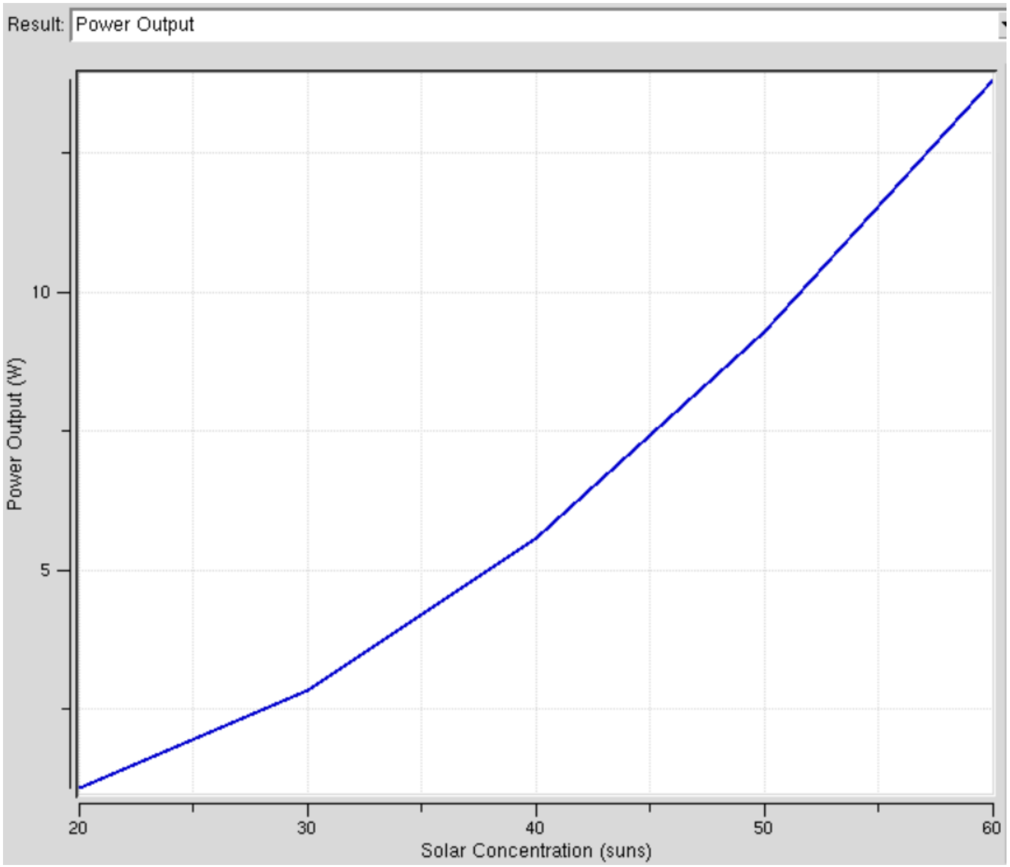


*Figure 29: Output Plot Example*

## 4.5: How to Create a Tool

### 4.5.1: NanoHUB

The simulation tool is run on NanoHUB.org. NanoHUB is a science and engineering hub mainly aimed towards the field of nanotechnology. It is used by scientists and engineers worldwide for research and education and is maintained by Purdue University.

### 4.5.2: Rappture Toolkit

Rappture Toolkit is an open-source application that was released in 2005. With Rappture, one can easily develop quick and powerful scientific applications with various underlying software languages which are listed in Table 2 below.

| | |
|---|---|
| MATLAB | Java |
| C | Python |
| C++ | Ruby |
| Octave | Fortran 77 |
| Tcl | Perl |

*Table 2: Rappture Support Languages*

### 4.5.3: Rappture Builder

To build a tool, user must learn to navigate Workspace, which is a Linux based Terminal developed by Nanonhub using a few commands shown below.

In the figure below, at the home terminal, by typing “ls”, a list of all files at the current directory are displayed.

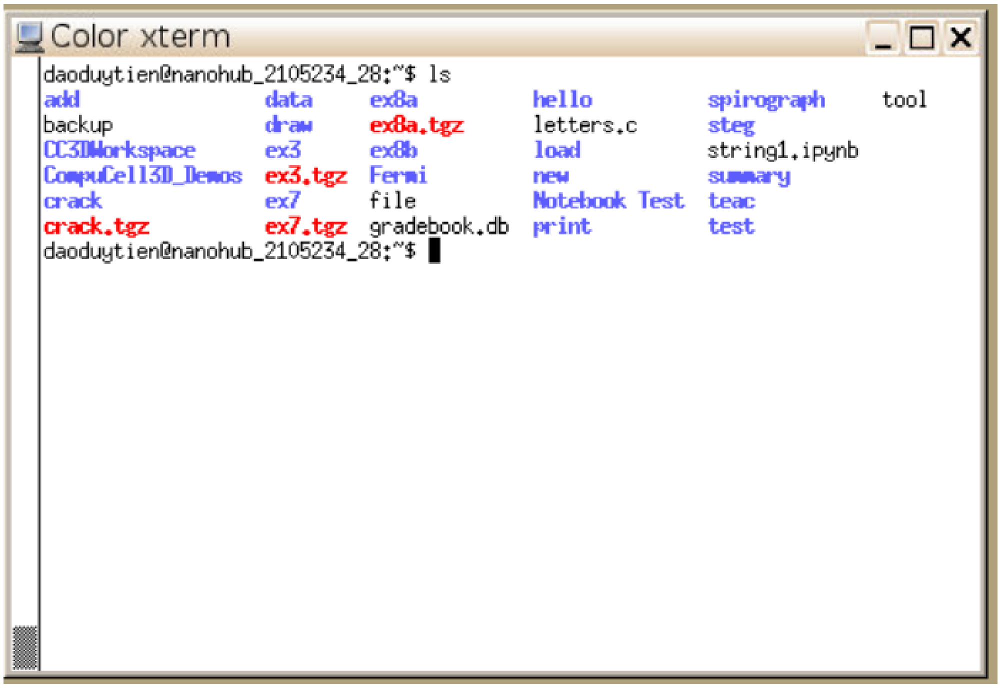


*Figure 30: List of Current Directory*

A test directory was created by entering “mkdir test”.

To move between directory, enter the command “cd” + directory name. “cd test” is entered to move to the “test” directory.

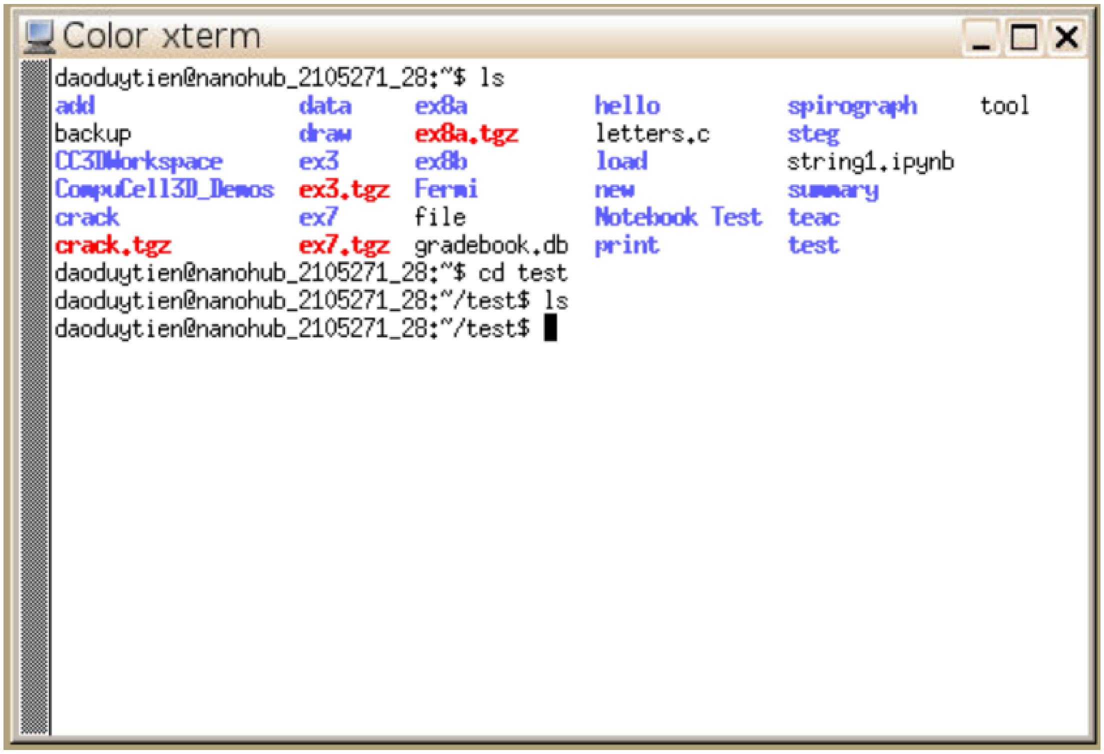


*Figure 31: Test Directory*

A tool can be built in the “test” directory by typing the command “rapture -builder” as shown below.

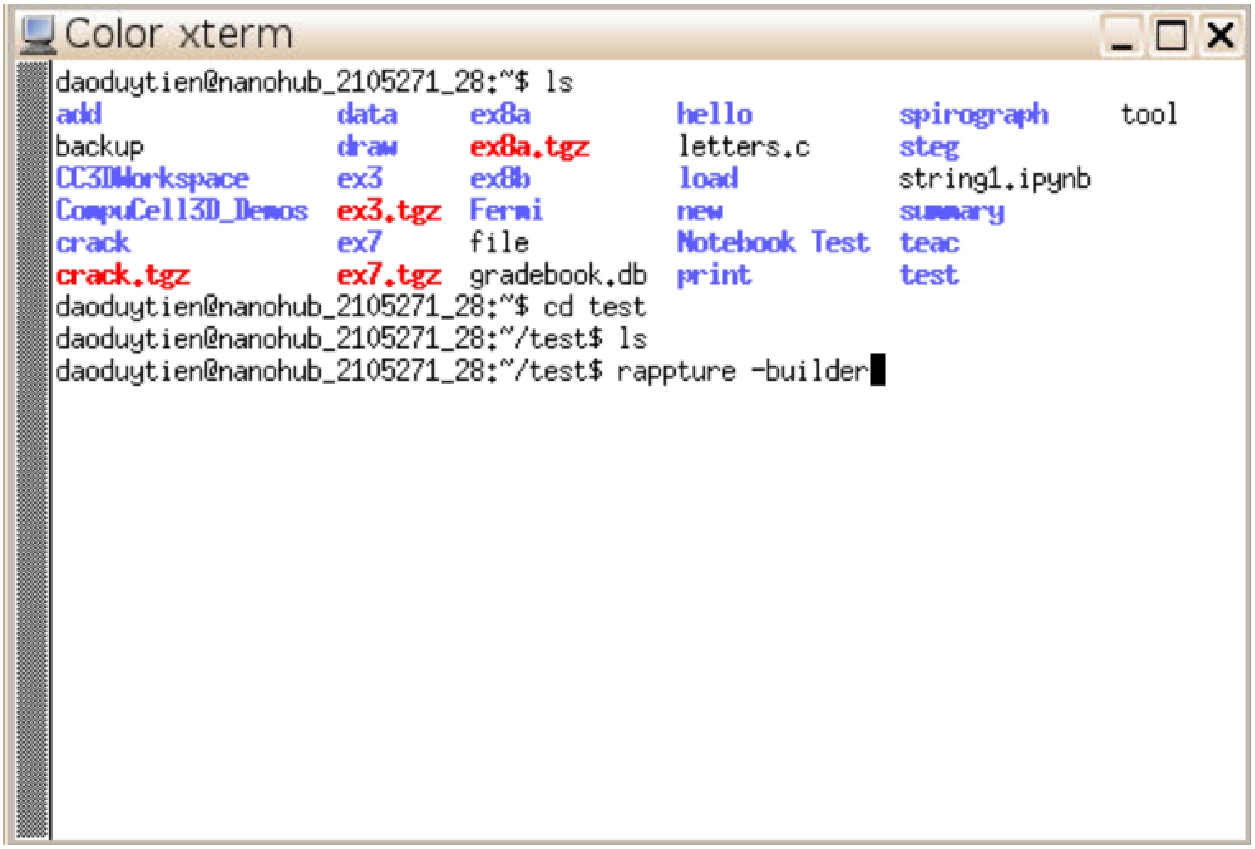


*Figure 32: Rappture Builder Example*

A display will show up that allows users to input objects for their tool.

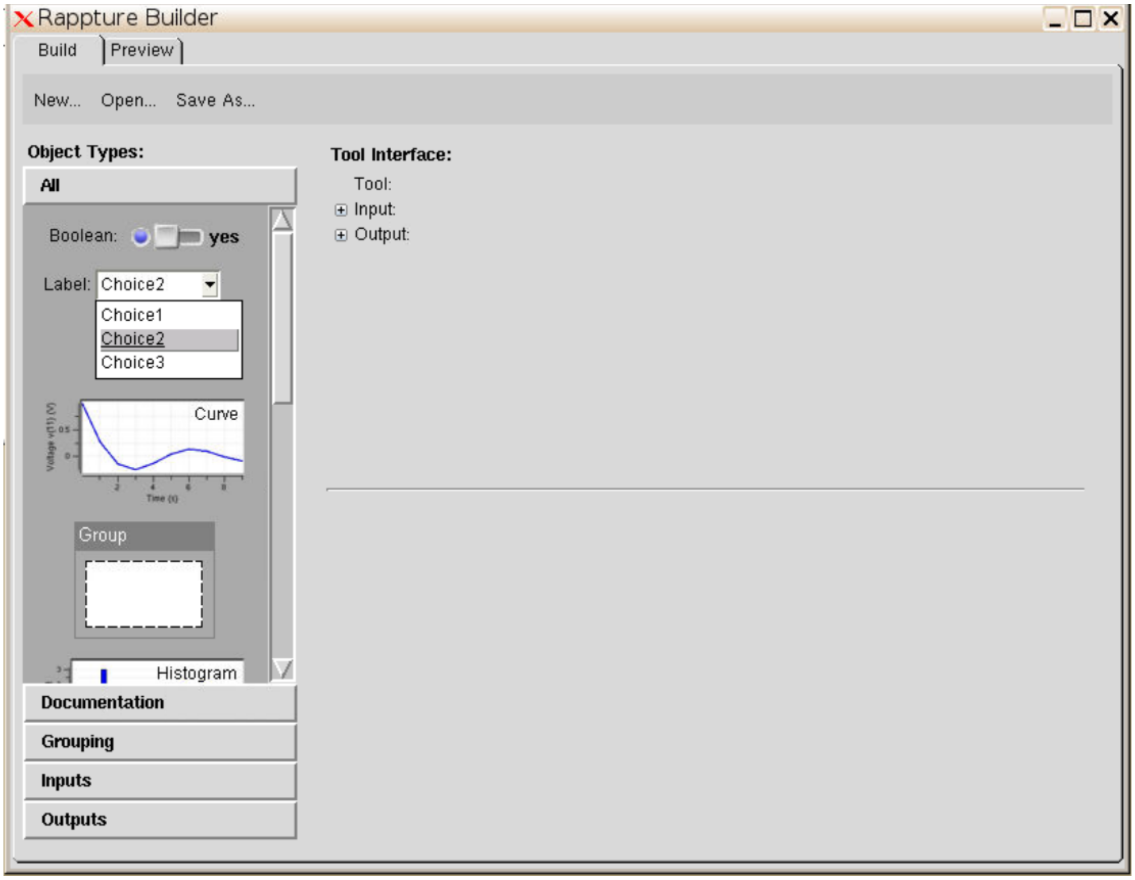


*Figure 33: User Input Objects*

The Builder is where the developers create their tool. In the figure above, the developers can simply click and drag what they object they would like to have on their simulator from the left tab into the Tool Interface. On the Tool Interface, developers can add inputs such as default value and descriptions of the object in the appropriate boxes. Developers can also choose which programming language they intend to use as the backbone of their simulation by selecting the appropriate tabs. An example of the objects displayed is shown in Figure 34. In Figure 34, MATLAB is chosen but can be any of the languages in Table 2.

Developers can preview what the interface of their simulator will look like based on the objects entered by selecting "Preview" in the top left corner of the screen.

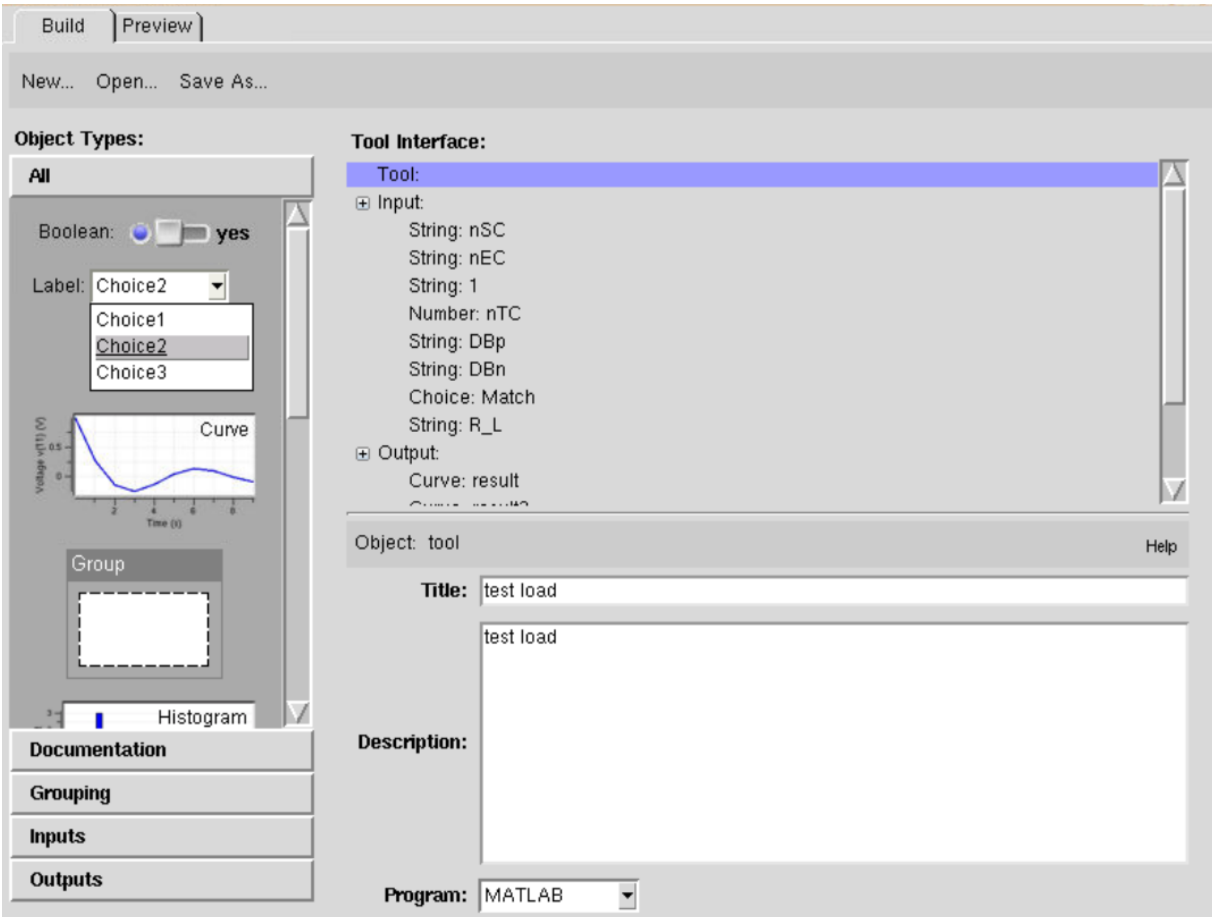


*Figure 34: Builder Example*

A preview of the interface is shown in Figure 35.

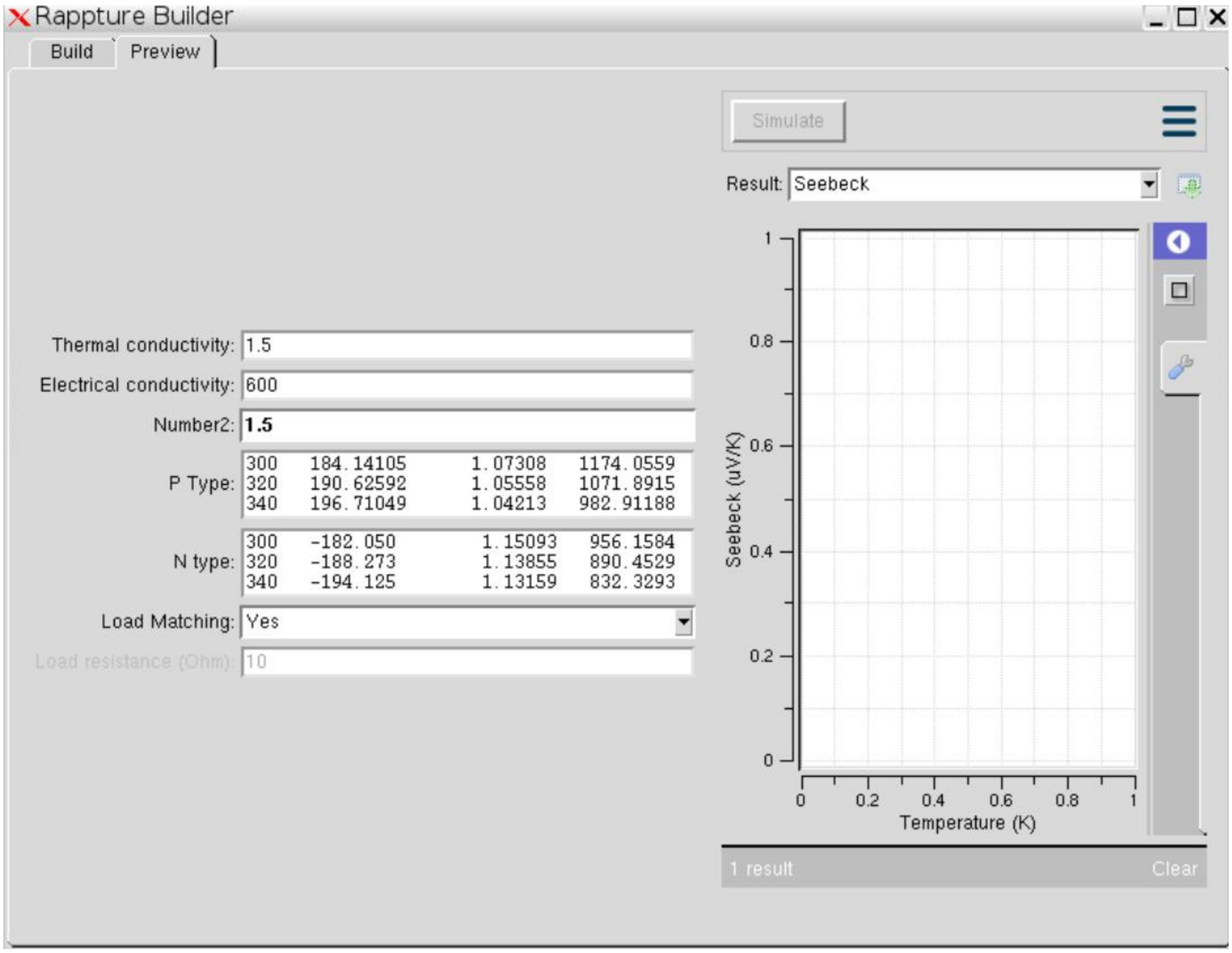


*Figure 35: Preview Interface Example*

Once the developers are satisfied with their layout, they can select “Save As” in figure 36.

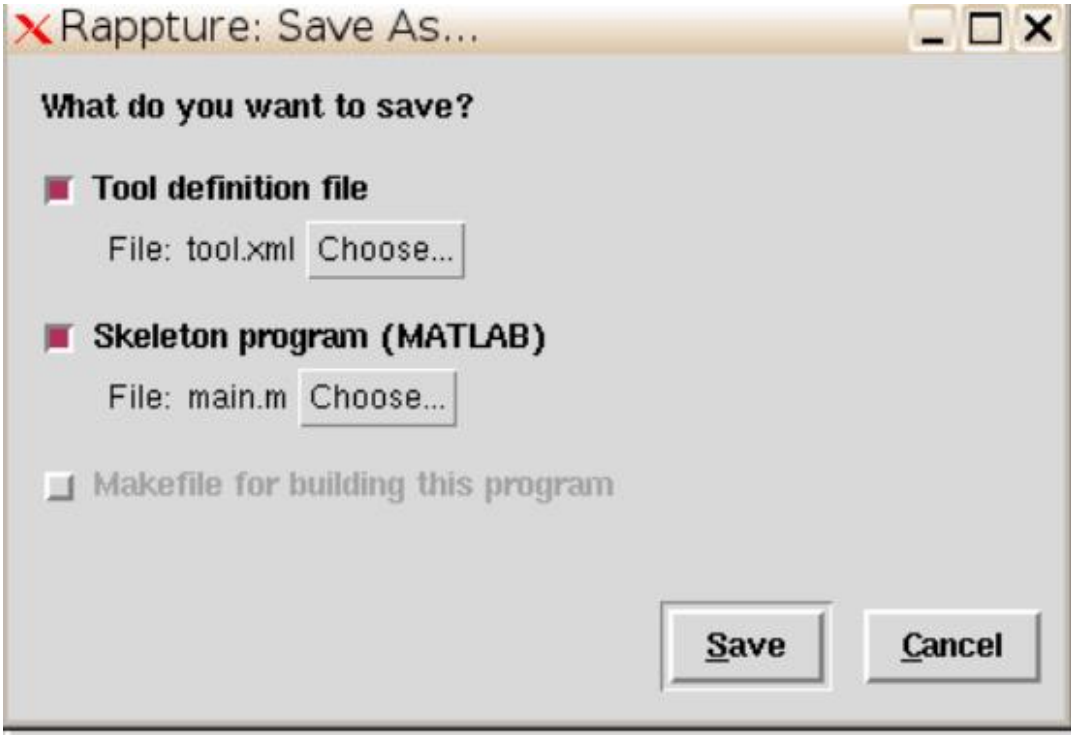


*Figure 36: Save As Screen*

Developers can choose to change the names of their tool and skeleton file and save. Saving the build will generate two files shown in Figure 37. The tool.xml file is the display and the main.m file works behind the scenes to run the algorithm for the simulation.

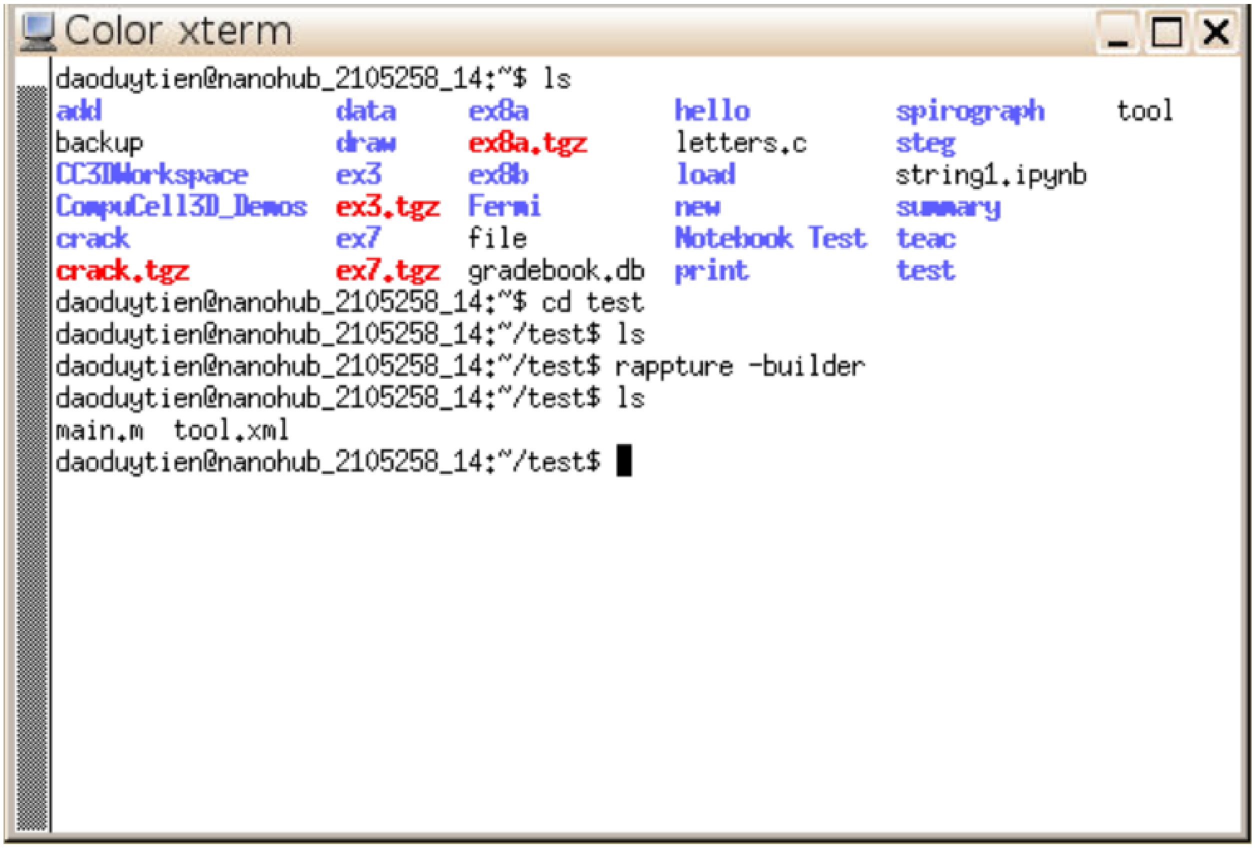


*Figure 37: Rappture Builder Output*

Users can choose to edit their tool.xml and main.m code by typing the command “gedit tool.xml” or “gedit main.m”. The tool can be run by typing the command “rappture” on the terminal.

For some tools, such as solarte, uploading data from the user are sometimes required to run the simulation, in this situation, a loader is necessary. Information on loader and other Nanohub capabilities can be found in the link in the References section below.

### 4.5.4: Tool Registration

Once the user is satisfied with their tool developed in Linux, their tool can be published. To publish their tool, the developers must register their tool with nanoHUB detailing what the tool is intended to do.

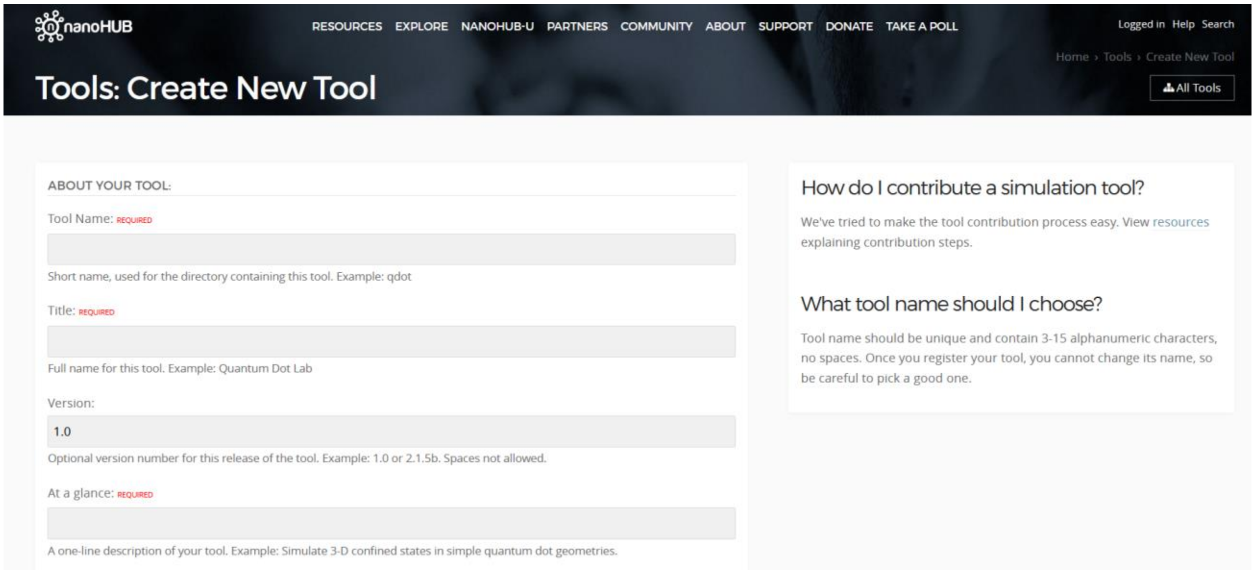


*Figure 38: Tool Registration [25]*

### 4.5.5: Subversion

Once the tool is registered, nanoHUB will inquire you to download a version control software such as Subversion or TortoiseSVN. Version control is the practice of tracking and managing software code, it allows developers to track changes over time by keeping track of every modification to the code in a database and revert to earlier version if necessary [26]. Other examples of version control include CVS and Git.


*Figure 39: Version Control Examples [27][28]*

Examples of Subversion files are shown below, here, the code main.m and tool.xml and all the associated files needed to run the tool are downloaded from Workspace and committed to NanoFORGE, the repository owned by Nanohub. The green checkmarks shows that the files have successfully committed and are up to date with nanoFORGE,

| Name | Date modified | Type | Size |
|---|---|---|---|
| bin | 2/23/2022 7:36 PM | File folder | |
| data | 2/23/2022 7:36 PM | File folder | |
| doc | 2/23/2022 7:36 PM | File folder | |
| middleware | 2/25/2022 2:14 PM | File folder | |
| rappture | 9/29/2022 1:34 PM | File folder | |
| src | 10/15/2022 1:03 PM | File folder | |
| .git-commit | 2/23/2022 7:36 PM | GIT-COMMIT File | 1 KB |

*Figure 40: Subversion Example Files*

In the figure below, once all the necessary files are committed to nanoFORGE, developers can choose to test run their tool by selecting “Launch Tool”. If the user is satisfied with their tool, they can select to publish the tool by approving it. If the user is unsatisfied with their tool, they can go back to their main.m or tool.xml file to make modifications, commit, and select “I’ve committed new code” to install your new codes and test run again.

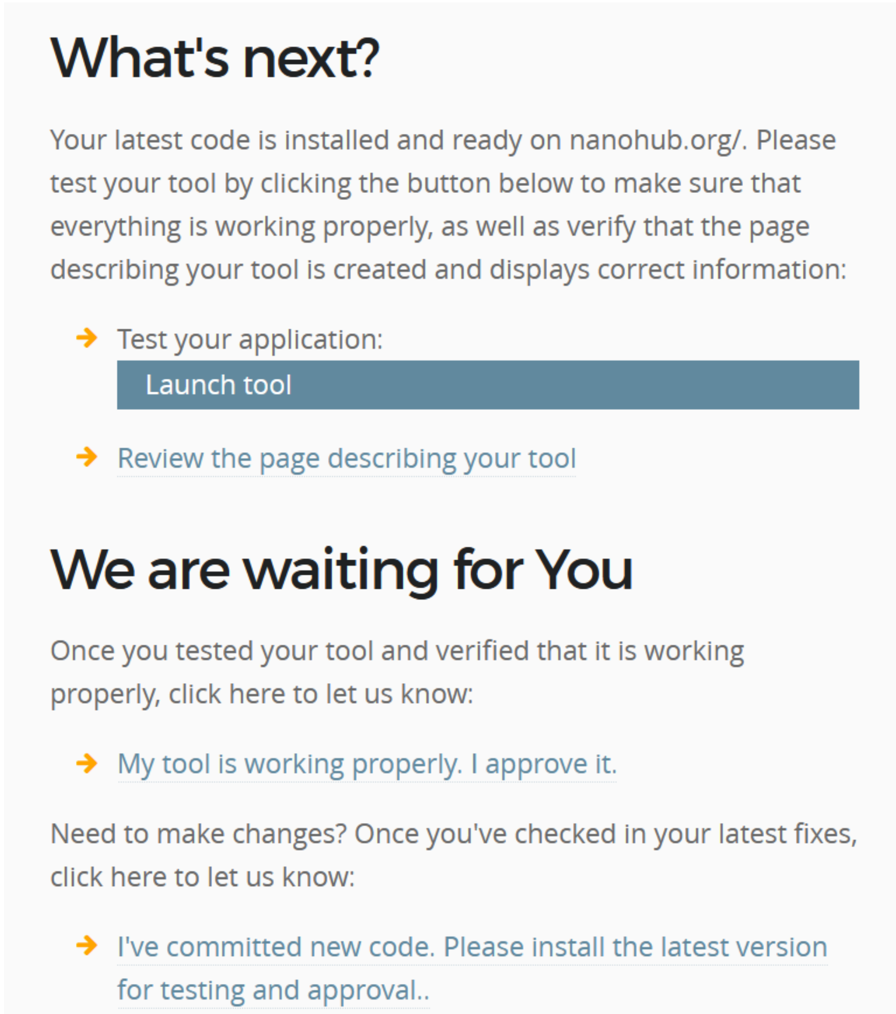

## What's next?

Your latest code is installed and ready on nanohub.org/. Please test your tool by clicking the button below to make sure that everything is working properly, as well as verify that the page describing your tool is created and displays correct information:

- Test your application:
  Launch tool
- Review the page describing your tool

## We are waiting for You

Once you tested your tool and verified that it is working properly, click here to let us know:

- My tool is working properly. I approve it.

Need to make changes? Once you've checked in your latest fixes, click here to let us know:

- I've committed new code. Please install the latest version for testing and approval..

*Figure 41: Publication Page*

# 5. Results and Discussions

## 5.1: Independent Variable: Solar Concentrations

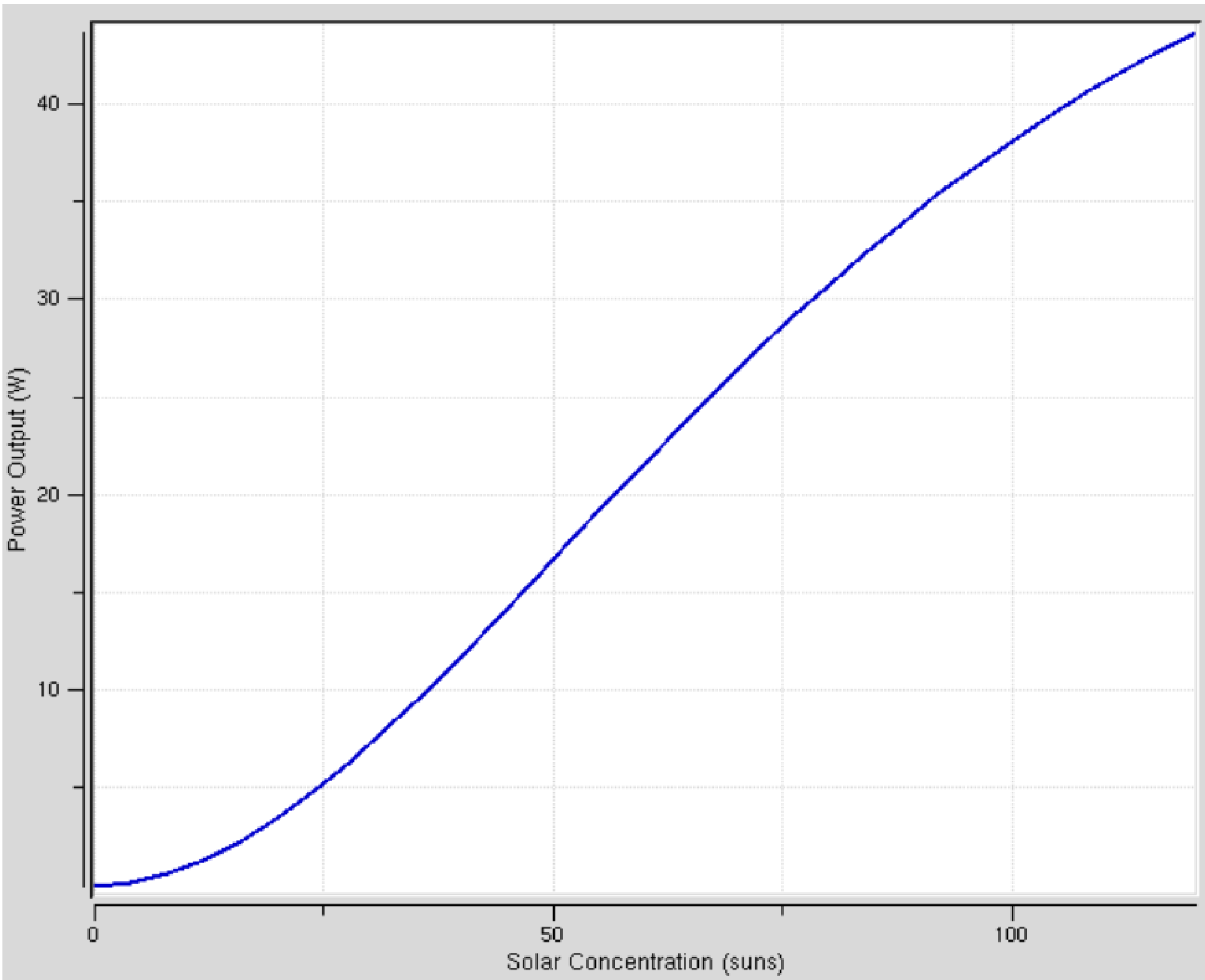


*Figure 42: Power Output Varying Solar Concentrations*

*TE Material: N and P-type Bismuth Telluride, Solar Concentrations: 0 – 120 suns, N and P-type Area: 4 $mm^2$,Leg Thickness: 3 mm, Fill Factor: 0.2, Solar Energy input from the Sun: 700 $W/m^2$, Transmittance through the Concentrator: 0.94, Conductive Hot-side Heat Transfer Coefficient: 5000 $W/m^2K$, Convective Hot-side Heat Transfer Coefficient: 20 $W/m^2K$, Solar Absorber Area: 100 $cm^2$, Absorber Absorbance: 0.9, Absorber Emissivity: 0.15, Contact Resistance: 0 Ohm, Thermal Conductivity of Gap Filler: 0.4 W/mK, Conductive Cold-side Heat Transfer Coefficient: 3000 $W/m^2K$, Ambient Temperature: 300 $^oK$, Load Matching Condition*

When running simulation with values set at default and typical cross-sectional area of 2x2 $mm^2$ used in commercial modules. Bismuth Telluride as n and p type elements are used as TE material and Solar Concentration were set as the independent variable from 0 – 120 suns. The results are shown in Figure 42 above. While the power output was expected to rise indefinitely due to the constantly increasing sun light and therefore temperature difference, the power output slow down past 120 suns. This is due to an increase in temperature which causes a decrease in electrical conductivity, thereby increasing the electrical resistance shown in the equation below

$$R = \frac{1}{G} = \frac{1}{\sigma}\frac{L}{A} \quad (52)$$

contributing to the power output which is explained by

$$P_{\text{out,max}} = N\frac{S^2(\Delta T)^2}{4R} \quad (53)$$

However, while decreasing electrical conductivity does contribute to the increase in electrical resistance, the effect is minimal compared to the temperature difference. A better explanation is that as temperature increase past the highest ZT point of Bismuth Telluride (~600 $^oK$), ZT decrease significantly, causing efficiency and power output to eventually decrease. This is evidenced by Figure 43 showing the efficiency decrease after ~84 suns and the hot side temperature in Figure 44 showing the temperature at the hot side of the TE at ~ 630 $^oK$

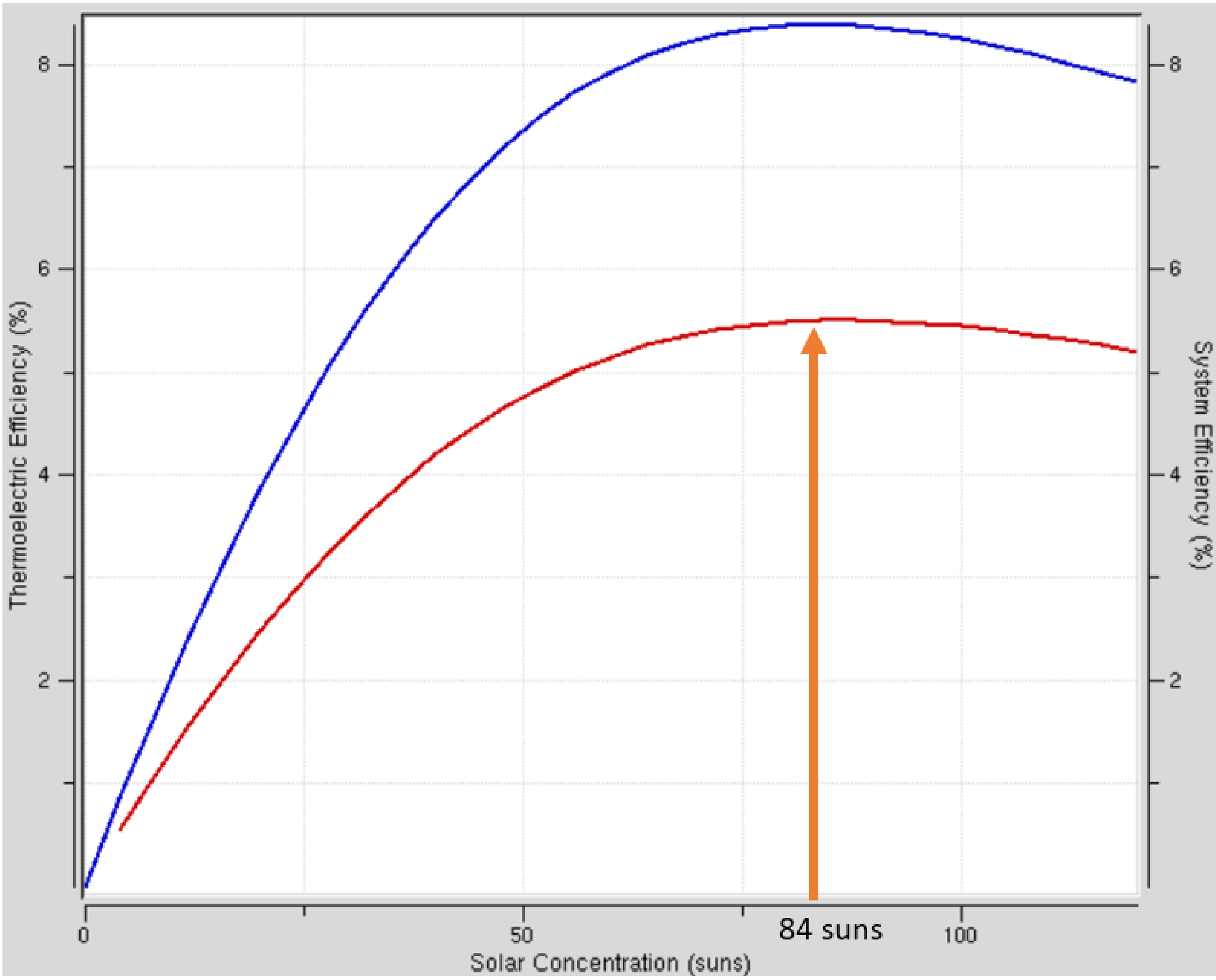


*Figure 43: TE and System Efficiency Varying Solar Concentrations*

*TE Material: N and P-type Bismuth Telluride, Solar Concentrations: 0 – 120 suns, N and P-type Area: 4 mm², Leg Thickness: 3 mm, Fill Factor: 0.2, Red line represents the system efficiency and blue line represents thermoelectric efficiency, Solar Energy input from the Sun: 700 W/m², Transmittance through the Concentrator: 0.94, Conductive Hot-side Heat Transfer Coefficient: 5000 W/m²K, Convective Hot-side Heat Transfer Coefficient: 20 W/m²K, Solar Absorber Area: 100 cm², Absorber Absorbance: 0.9, Absorber Emissivity: 0.15, Contact Resistance: 0 Ohm, Thermal Conductivity of Gap Filler: 0.4 W/mK, Conductive Cold-side Heat Transfer Coefficient: 3000 W/m²K, Ambient Temperature: 300 °K, Load Matching*

*Condition*

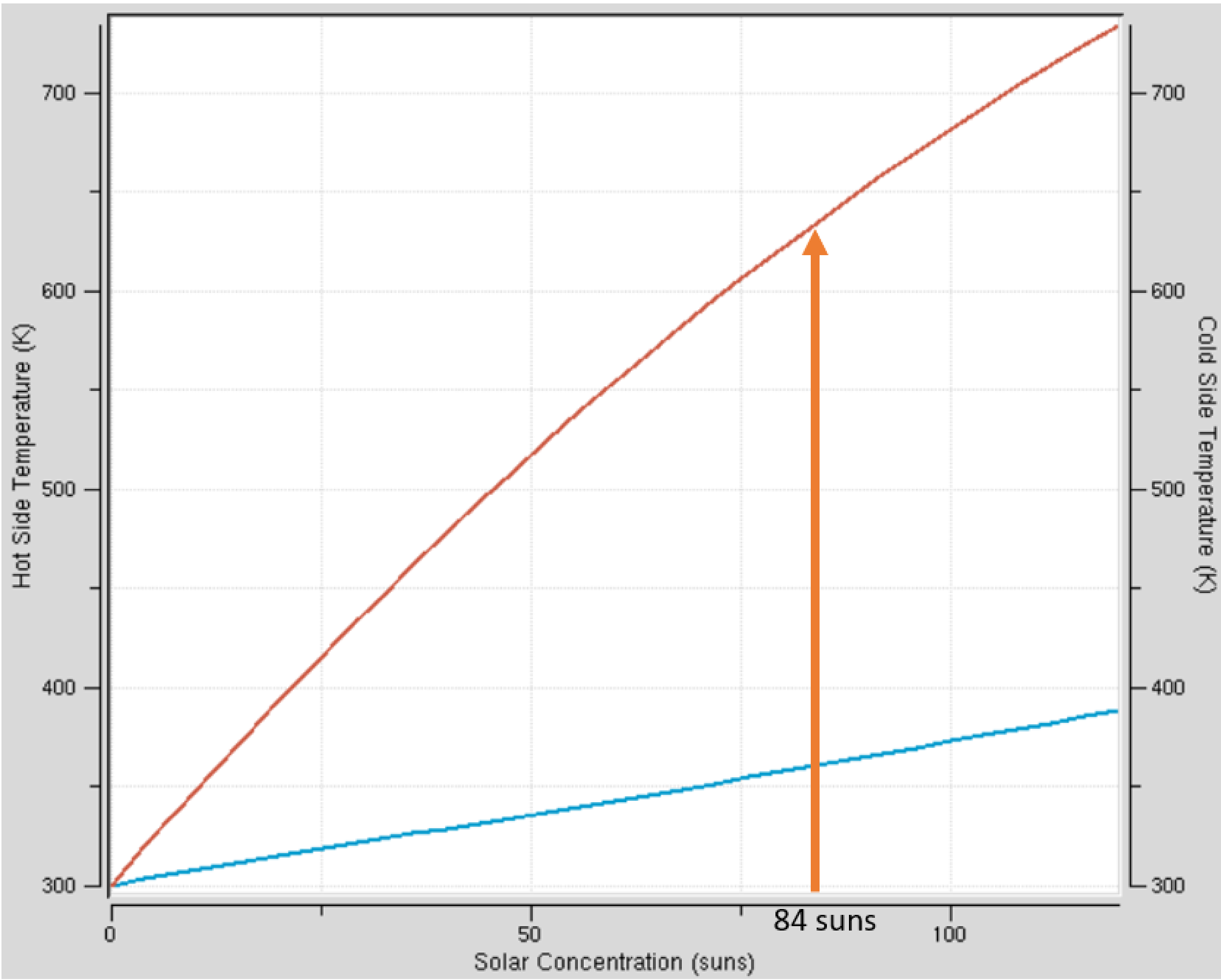


*Figure 44: Hot Side and Cold-side Temperature*

*TE Material: N and P-type Bismuth Telluride, Solar Concentrations: 0 – 120 suns, N and P-type Area: 4 mm$^2$, Leg Thickness: 3 mm, Fill Factor: 0.2, Red line represents the hot-side temperature and blue line represents cold-side temperature of the thermoelectric element leg, Solar Energy input from the Sun: 700 W/m$^2$, Transmittance through the Concentrator: 0.94, Conductive Hot-side Heat Transfer Coefficient: 5000 W/m$^2$K, Convective Hot-side Heat Transfer Coefficient: 20 W/m$^2$K, Solar Absorber Area: 100 cm$^2$, Absorber Absorbance: 0.9, Absorber Emissivity: 0.15, Contact Resistance: 0 Ohm, Thermal Conductivity of Gap Filler: 0.4 W/mK, Conductive Cold-side Heat Transfer Coefficient: 3000 W/m$^2$K, Ambient Temperature: 300 $^o$K, Load Matching Condition*

Figure 42-44 illustrates the simulation results of Bismuth Telluride as a solar TE material when running the solar concentrations as the independent variable. This tool is operating under the assumption that the material does not degrade over time or melts with high enough temperature. While the simulation here does not show the melting point of Bismuth Telluride (~800 ºK) [29], it is up to the engineer to understand the limits of their material and adjust as needed.

## 5.2: Independent Variable: Length of TE Elements

Using all default values in the input slide, Bismuth Telluride n and p-type as TE material, and the leg thickness as independent variable. Data was simulated, and the results were plotted below with respect to the independent variable as: Power Output, TE Efficiency, and System Efficiency in Figures 45 and 46 below.

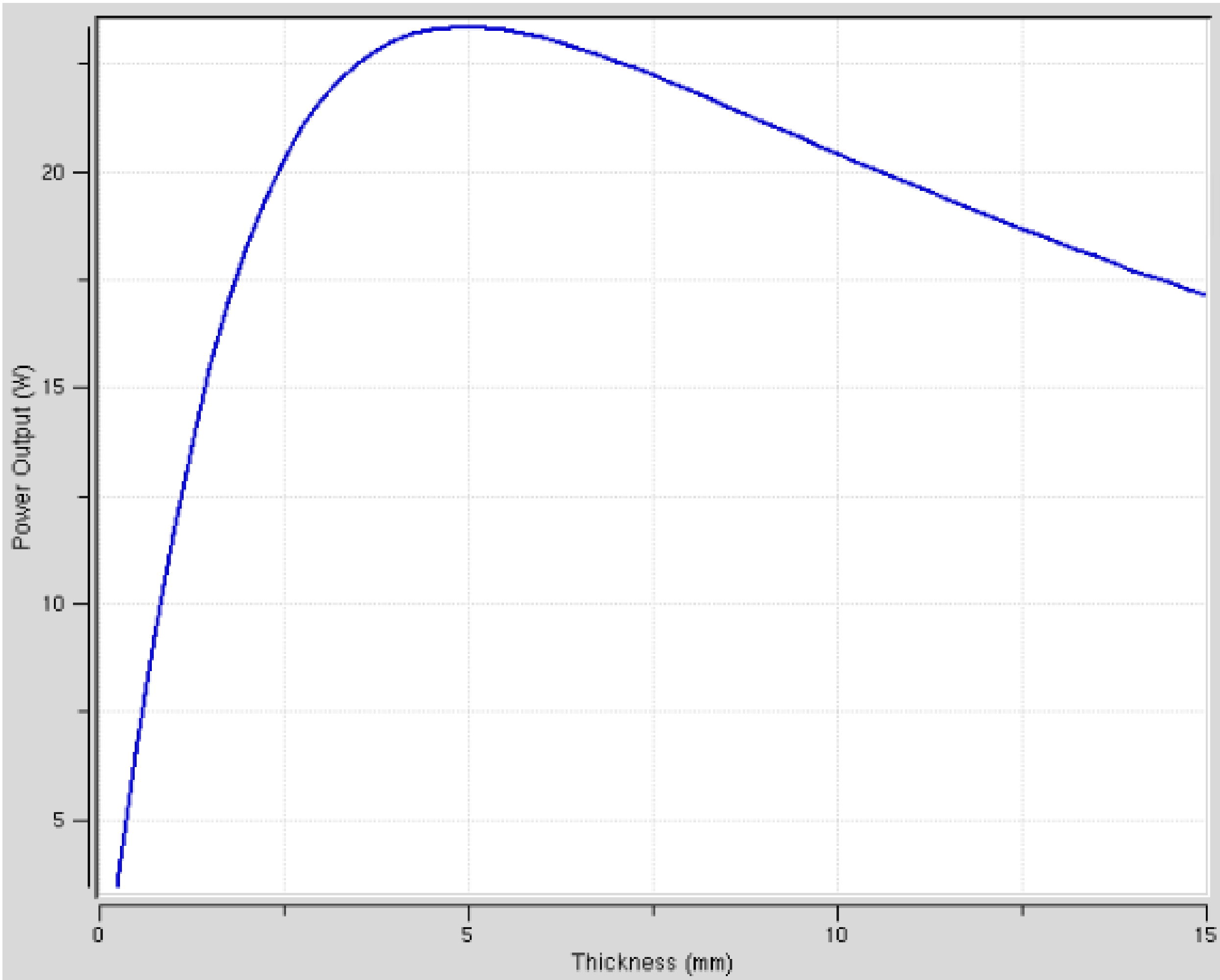


*Figure 45: Power Output Varying Length Thickness*

*TE Material: N and P-type Bismuth Telluride, Leg Thickness: 0 – 15 mm, Solar Concentrations: 60 suns, N and P-type Area: 4 mm$^2$, Fill Factor: 0.2, Solar Energy input from the Sun: 700 W/m$^2$, Transmittance through the Concentrator: 0.94, Conductive Hot-side Heat Transfer Coefficient: 5000 W/m$^2$K, Convective Hot-side Heat Transfer Coefficient: 20 W/m$^2$K, Solar Absorber Area: 100 cm$^2$, Absorber Absorbance: 0.9, Absorber Emissivity: 0.15, Contact Resistance: 0 Ohm, Thermal Conductivity of Gap Filler: 0.4 W/mK, Conductive Cold-side Heat Transfer Coefficient: 3000 W/m$^2$K, Ambient Temperature: 300 $^o$K, Load Matching Condition*

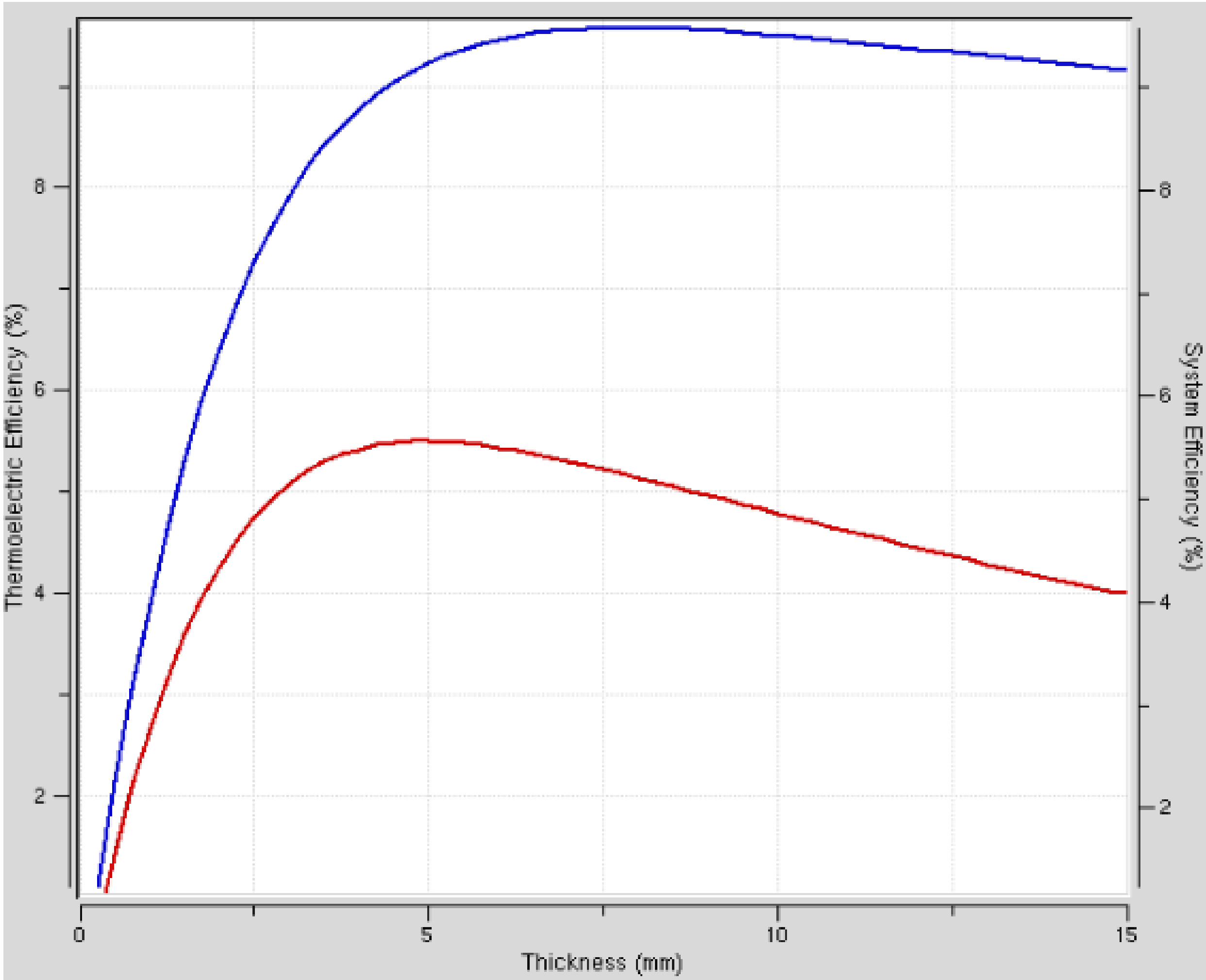


*Figure 46: TE and System Efficiency Varying Leg Thickness*

*TE Material: N and P-type Bismuth Telluride, Leg Thickness: 0 – 15 mm, Solar Concentrations: 60 suns, N and P-type Area: 4 $mm^2$, Fill Factor: 0.2, Solar Energy input from the Sun: 700 $W/m^2$, Transmittance through the Concentrator: 0.94, Conductive Hot-side Heat Transfer Coefficient: 5000 $W/m^2K$, Convective Hot-side Heat Transfer Coefficient: 20 $W/m^2K$, Solar Absorber Area: 100 $cm^2$, Absorber Absorbance: 0.9, Absorber Emissivity: 0.15, Contact Resistance: 0 Ohm, Thermal Conductivity of Gap Filler: 0.4 W/mK, Conductive Cold-side Heat Transfer Coefficient: 3000 $W/m^2K$, Ambient Temperature: 300 °K, Load Matching Condition*

Like the power output in section 5.1. Power output in Figure 45 is explained by an increase in the temperature difference between the hot and cold side, but power output is dampened by the increase in electrical resistance by the equation 52.

Resistance increases with respect to length. Therefore, as length increase, resistance will be a greater and greater factor, at the same time, thermal resistance, which is calculated as

$$R_{TH} = \frac{1}{K} = \frac{1}{k}\frac{L}{A} \quad (54)$$

also increases, making the temperature on the top side harder to move down the cold side, creating a higher temperature as length increases. However, electrical resistance will eventually overtake temperature difference as the dominant factor in contributing to the power output, shown in Figure 45.

## 5.3: Independent Variable: Fill Factor of TE Elements

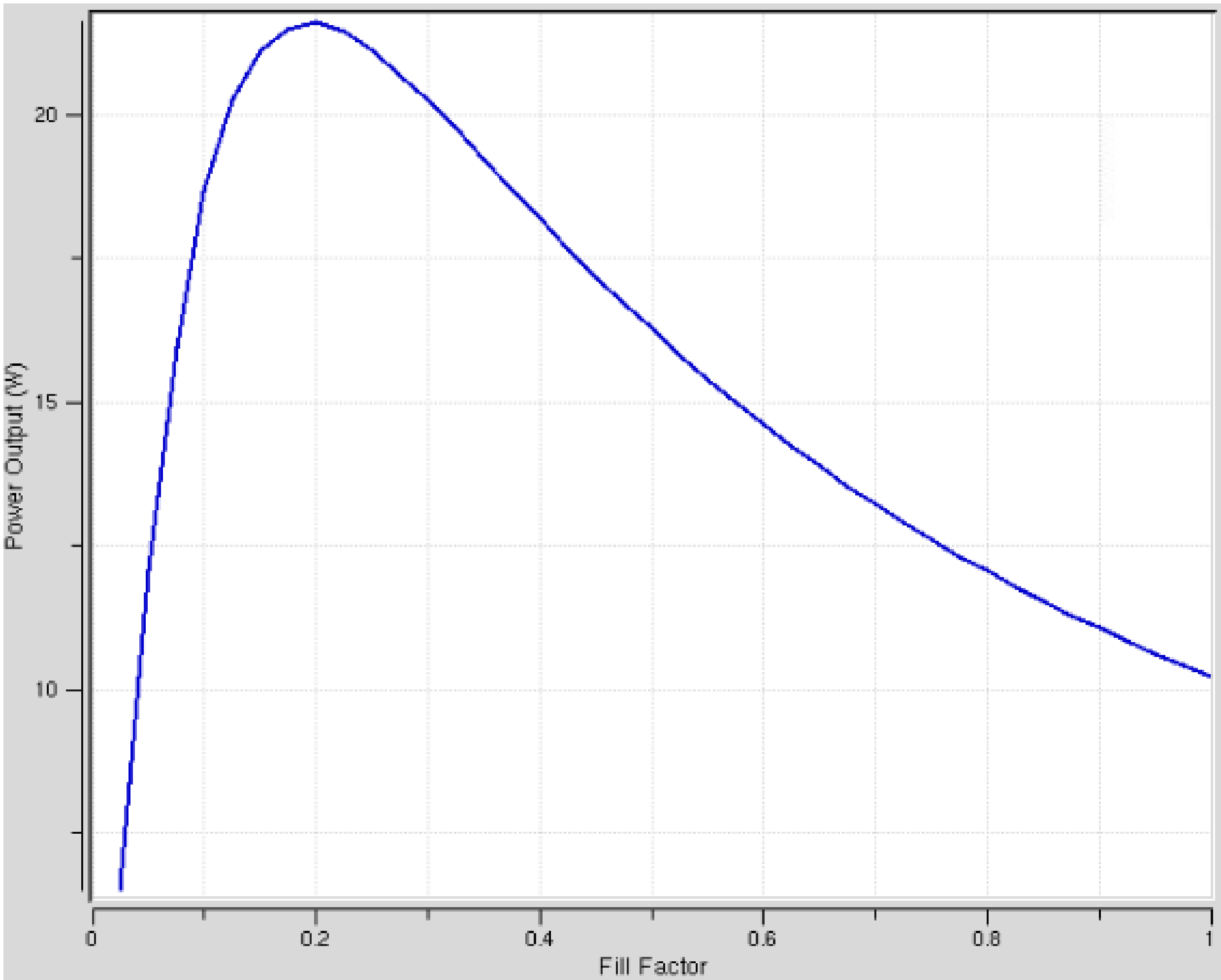


*Figure 47: Power Output Varying Fill Factor*

*TE Material: N and P-type Bismuth Telluride, Fill Factor: 0.1 – 1, Solar Concentrations: 60 suns, N and P-type Area: 4 mm², Leg Thickness: 3 mm, Solar Energy input from the Sun: 700 W/m², Transmittance through the Concentrator: 0.94, Conductive Hot-side Heat Transfer Coefficient: 5000 W/m²K, Convective Hot-side Heat Transfer Coefficient: 20 W/m²K, Solar Absorber Area: 100 cm², Absorber Absorbance: 0.9, Absorber Emissivity: 0.15, Contact Resistance: 0 Ohm, Thermal Conductivity of Gap Filler: 0.4 W/mK, Conductive Cold-side Heat Transfer Coefficient: 3000 W/m²K, Ambient Temperature: 300 °K, Load Matching Condition*

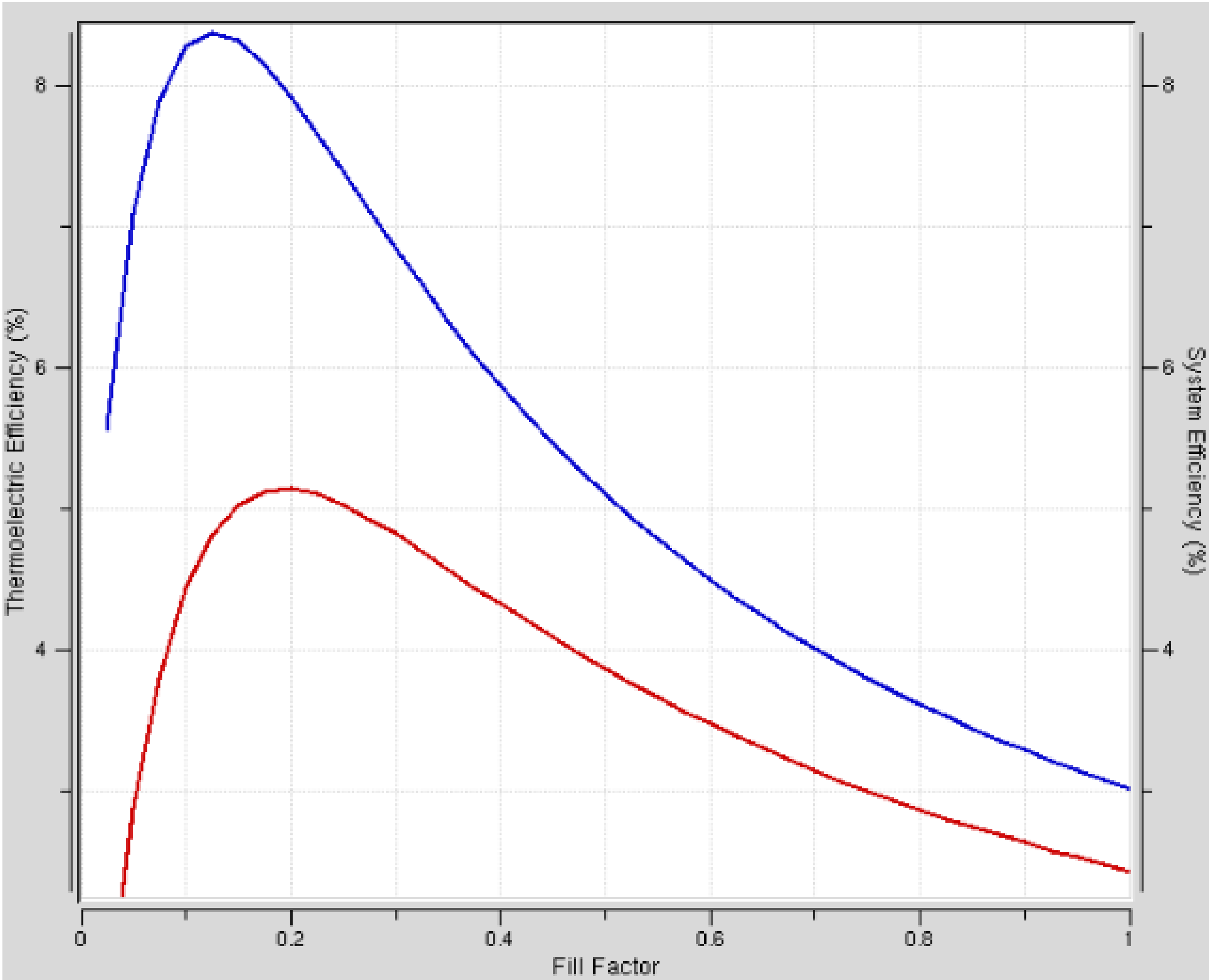


*Figure 48: TE and System Efficiency Varying Fill Factor*

*TE Material: N and P-type Bismuth Telluride, Fill Factor: 0.1 – 1, Solar Concentrations: 60 suns, N and P-type Area: 4 mm², Leg Thickness: 3 mm, Solar Energy input from the Sun: 700 W/m², Transmittance through the Concentrator: 0.94, Conductive Hot-side Heat Transfer Coefficient: 5000 W/m²K, Convective Hot-side Heat Transfer Coefficient: 20 W/m²K, Solar Absorber Area: 100 cm², Absorber Absorbance: 0.9, Absorber Emissivity: 0.15, Contact Resistance: 0 Ohm, Thermal Conductivity of Gap Filler: 0.4 W/mK, Conductive Cold-side Heat Transfer Coefficient: 3000 W/m²K, Ambient Temperature: 300 °K, Load Matching Condition*

When Fill Factor is the independent variable, the Fill Factor equation is used

$$F = \frac{N_{TE}(A_n + A_p)}{A_{\text{total}}} \quad (55)$$

In this situation, n and p type area remained fixed, $N_{TE}$ changes proportionally to fill factor. When fill factor increases, more $N_{TE}$ parallel leg creates more heat channel across the TE, causing the total thermal resistance to decrease. With less thermal resistance, heat can more effectively flow down the TE to the cold side, causing a lower temperature difference.

Therefore, in Figure 47, Power output is seen only increasing between fill factor 0 ~ 0.20 before decreasing when $\Delta T$ becomes the dominating factor.

## 5.4: Data Optimization for Maximum System Efficiency

Lastly, using the 3 independent variables shown above, we can use the tool to optimize for various output such as: power, system efficiency, cost, etc., Optimizing for system efficiency is chosen as the primary output and later cost is chosen to determine the best parameters that would give homeowners the best return on their investment as system efficiency accounts for energy generated as well as energy used for generation, all of which determines the cost of the solar TE system.

Using the data from Figure 43, the max System Efficiency is found to be at 84 suns using default values in the tool and 2x2 $mm^2$ cross-sectional area which is standard for commercial TE module.

Next, we set 84 suns and 2x2 $mm^2$ as our user input data while the rest is at default values and vary TE length from 1 – 15 mm, changing the fill factor by 0.1 after every simulation until the fill factor of 1.0. The result is shown below as superimposed data.

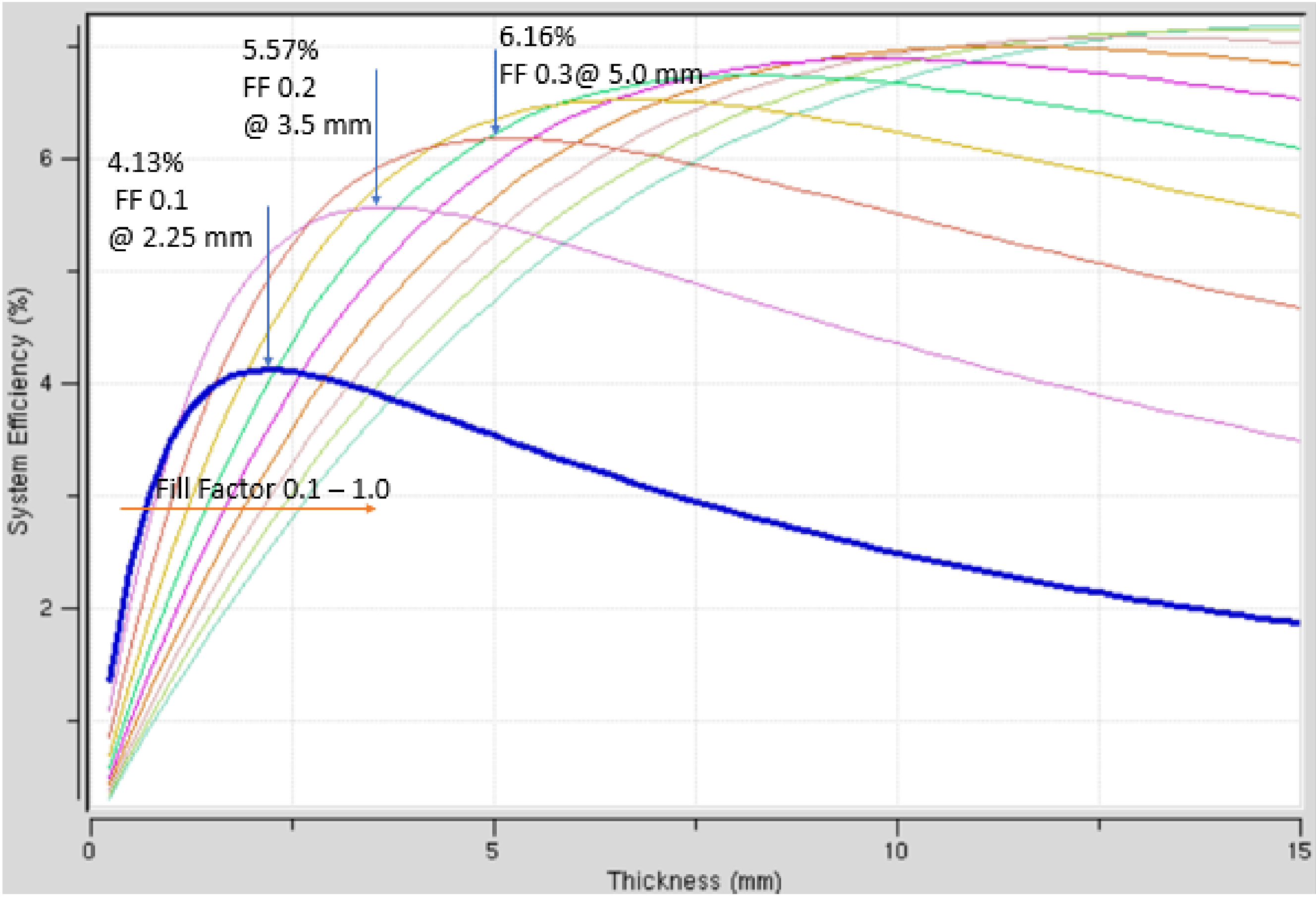


*Figure 49: Vary Thickness Optimize Fill Factor System Efficiency*

*TE Material: N and P-type Bismuth Telluride, Leg Thickness: 0 – 15 mm, Fill Factor: 0.1 – 1, Solar Concentrations: 84 suns, N and P-type Area: 4 mm$^2$, Solar Energy input from the Sun: 700 W/m$^2$, Transmittance through the Concentrator: 0.94, Conductive Hot-side Heat Transfer Coefficient: 5000 W/m$^2$K, Convective Hot-side Heat Transfer Coefficient: 20 W/m$^2$K, Solar Absorber Area: 100 cm$^2$, Absorber Absorbance: 0.9, Absorber Emissivity: 0.15, Contact Resistance: 0 Ohm, Thermal Conductivity of Gap Filler: 0.4 W/mK, Conductive Cold-side Heat Transfer Coefficient: 3000 W/m$^2$K, Ambient Temperature: 300 °K, Load Matching Condition*

By reviewing the data output, we determined the max system efficiency at fill factor 0.1 – 0.3 which are shown in Figure 49. While max efficiency at fill factor 0.4 – 1.0 can be determine, to achieve the maximum efficiency, increasing leg thickness would also increase material cost at a much higher rate than efficiency and therefore not feasible.

In Figure 49, the maximum system efficiency increases by 34.87% from fill factor 0.1 to 0.2 while the max efficiency only increases by 10.59% from fill factor 0.2 to 0.3, this makes fill factor 0.2 the ideal choice for maximum system efficiency and 0.1 as the next logical choice.

Material Cost/Watt is then calculated to the determine the fill factor that gives the best efficiency and also accounting for the best cost. The equation for material Cost/Watt is calculated as

$$\frac{(N_p + A_p + L_p) + (N_n + A_n + L_p) * Material\ Density * Cost/kg}{P_{out}} \quad (56)$$

with material density of 7.7 g/cm$^3$ [29] and powder Bismuth Telluride at \$100.00/kg [30]

Figure 50 displays the cost by varying leg thickness and changing fill factor after every simulation. The figure shows that the cost to implement optimization parameters for fill factor 0.2 is more than 2 times more expensive the 0.1. This makes fill factor 0.1 as the best choice for homeowners to choose when determining the best system efficiency for their money at the cost of \$0.07/Watt. However, at the cost of only \$0.16/Watt, fill factor of 0.2 should not be ignored if the homeowners decide to spend a little bit more for a better efficiency.

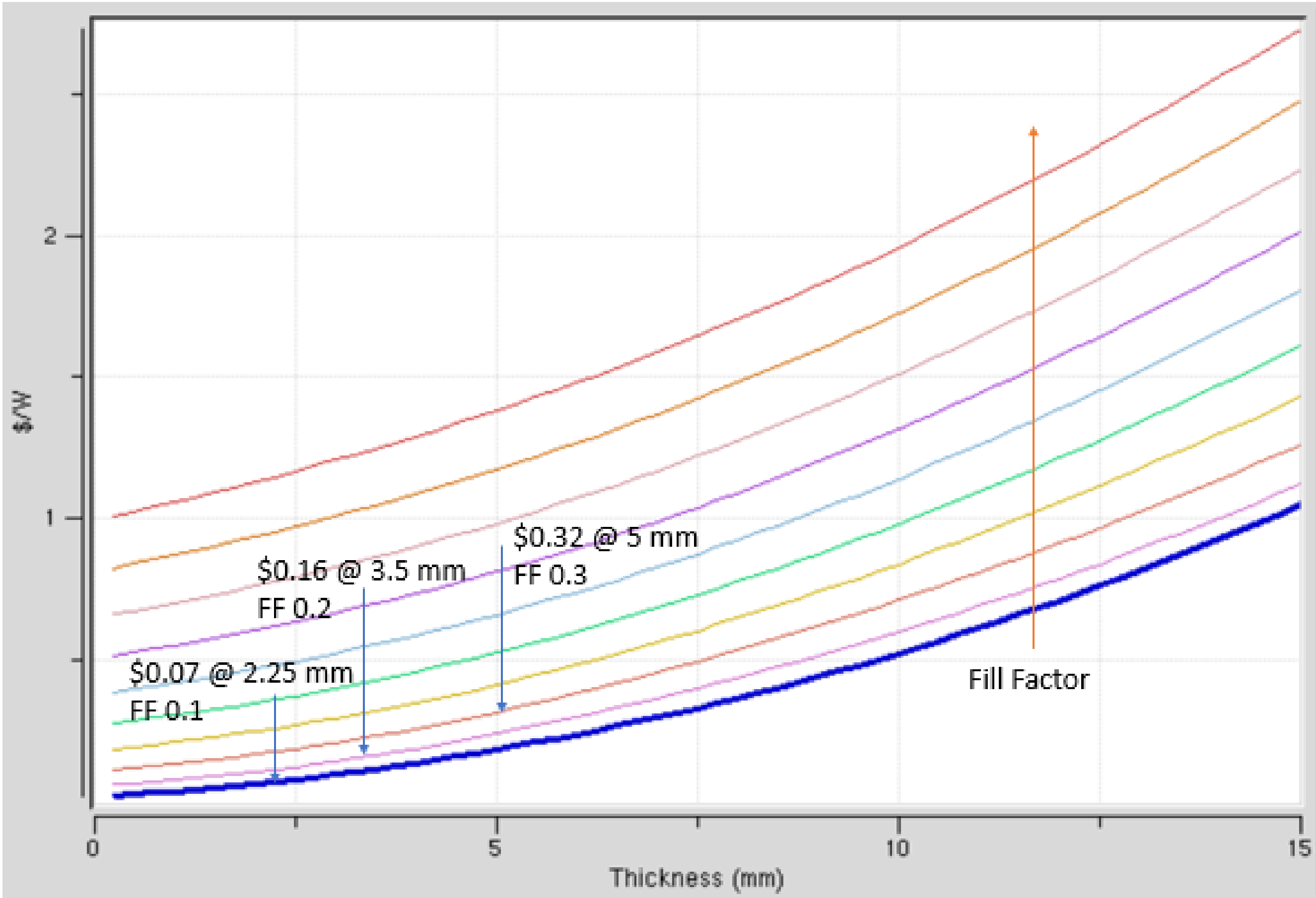


*Figure 50: Optimize Cost/Watt*

*TE Material: N and P-type Bismuth Telluride, Leg Thickness: 0 – 15 mm, Fill Factor: 0.1 – 1, Solar Concentrations: 84 suns, N and P-type Area: 4 mm$^2$, Bismuth Telluride Density: 7.7 g/cm$^3$ , Bismuth Telluride Cost: \$100.00/kg, Solar Energy input from the Sun: 700 W/m$^2$, Transmittance through the Concentrator: 0.94, Conductive Hot-side Heat Transfer Coefficient: 5000 W/m$^2$K, Convective Hot-side Heat Transfer Coefficient: 20 W/m$^2$K, Solar Absorber Area: 100 cm$^2$, Absorber Absorbance: 0.9, Absorber Emissivity: 0.15, Contact Resistance: 0 Ohm, Thermal Conductivity of Gap Filler: 0.4 W/mK, Conductive Cold-side Heat Transfer Coefficient: 3000 W/m$^2$K, Ambient Temperature: 300 $^o$K, Load Matching Condition*

Furthermore, Figure 51 shows a similar power output increase of 34.95% from fill factor 0.1 to fill factor 0.2 and a 11.09% increase from 0.2 to 0.3, making fill factor 0.1 as the optimal fill factor for best system efficiency while also managing cost and fill factor 0.2 as the alternative option for higher efficiency and power output for twice the material cost.

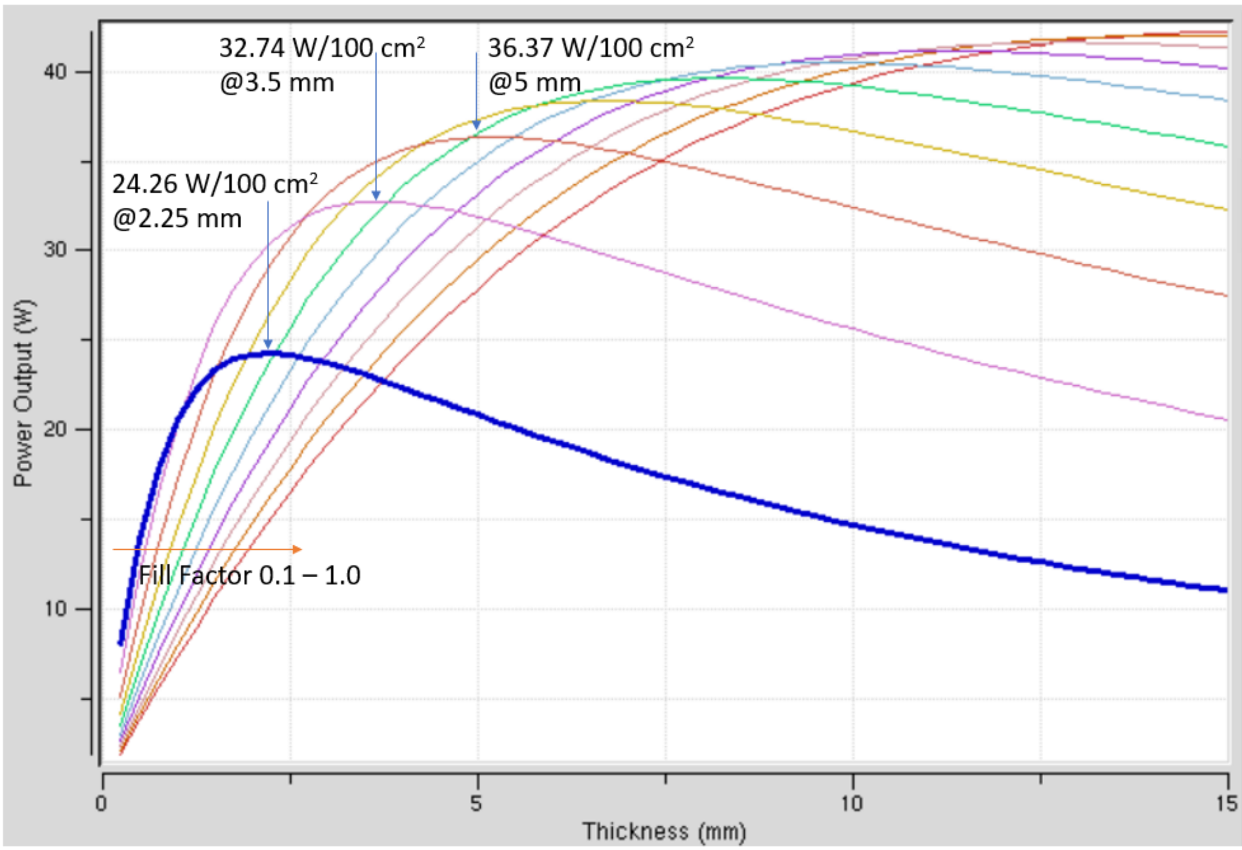


*Figure 51: Optimize Power Output*

*TE Material: N and P-type Bismuth Telluride, Leg Thickness: 0 – 15 mm, Fill Factor: 0.1 – 1, Solar Concentrations: 84 suns, N and P-type Area: 4 mm$^2$, Solar Energy input from the Sun: 700 W/m$^2$, Transmittance through the Concentrator: 0.94, Conductive Hot-side Heat Transfer Coefficient: 5000 W/m$^2$K, Convective Hot-side Heat Transfer Coefficient: 20 W/m$^2$K, Solar Absorber Area: 100 cm$^2$, Absorber Absorbance: 0.9, Absorber Emissivity: 0.15, Contact Resistance: 0 Ohm, Thermal Conductivity of Gap Filler: 0.4 W/mK, Conductive Cold-side Heat Transfer Coefficient: 3000 W/m$^2$K, Ambient Temperature: 300 $^o$K, Load Matching Condition*

The result above shows the maximize system efficiency one can achieve using the uploaded Bismuth Telluride n and p type material. While this tool is not a one-size-fits-all, running the tool with their own materials will give engineers a good idea of what to expect as in terms of power output, efficiency, and costs, etc., It is up to the homeowners and engineers to determine what is the best material and cost for their needs.

## 6. Conclusions and Future Work

The tool above demonstrated the ability to simulate energy harvesting based on temperature dependent thermoelectric material properties. In this tool, designers can simulate with 4 independent variables: cross-sectional area, leg thickness, solar concentrations, or fill factor. As demonstrated in section 5.4, it is up to the users to optimize their design to fit the needs of their situation. Aside from an already uploaded repository of thermoelectric properties data for commonly used TE materials such as Bismuth Telluride and Lead Telluride, designers can also upload their own TE materials properties by following the instruction shown in the tool. Changing each individual input values is also an option. By changing individual value, the algorithm will calculate based on the new values that the users set, these values range from the physical dimension of the TE element to the amount of solar input that is giving off by the sun, a full list is shown in the tool.

Simulation outputs give users a good idea of how much power they should be expecting in an ideal environment. Often times, maximum TE and system efficiency do not align with the maximum power output. In this situation, users must determine whether power must be sacrificed for efficiency or vice versa. For easy comparison, power output is plotted with respect to the independent variable, along with the aforementioned TE, system efficiency, and cost, etc.,

In our simulation, we chose to optimize for maximum system efficiency while also accounting for material cost/Watt. Using conventional TE material of Bismuth Telluride, which are often used for low-temperatures TE applications, we were able to optimize for system efficiency of

4.13% at the cost of \$0.07/Watt. While the cost may seem low, this does not account for the concentrator system, the cooling system, and everything else that also accounts for the whole system cost.

To compete with residential photovoltaic panels which have been shown to generate a \$/Watt price as low as \$2.71/Watt [31] for the residential PV system, new materials are needed to be developed that can work efficiently at high temperatures while also generating great power output. Fortunately, in the past decade, new TE materials, such as SnSe and PbTe, have shown great promise in tackling these problems at the mid to high temperature range (700$^{o}$K - 1000$^{o}$K) and further research are still being conducted to develop even better TE materials. All this is evidenced that it is now a great time to invest and research into the field of solar thermoelectric and thermoelectric as a whole.

Future work will need to be looked into the whole cost of the solar TE system as it will be more reflective of the whole cost of implementing solar TE. Reducing the cost of solar TE is also a big area to find ways to better develop materials and better effectively managing costs.

## Bibliography

[1] Gavan Walsh. “The Political Economy of Energy”. M.S. Thesis, University of Amsterdam, 2021.

[2] Elizabeth Morse, “Non-Renewable Energy”, *National Geographic*, [Online]. Available: https://education.nationalgeographic.org/resource/non-renewable-energy. [Accessed September 2022].

[3] Steve Hurley, “Opportunities for Solar Energy”, *Explaining Science*, 2021. [Online]. Available: https://explainingscience.org/2021/10/18/opportunities-for-solar-energy. [Accessed October 2022].

[4] “Photovoltaic Cell”, *Energy Education*. [Online]. Available: https://energyeducation.ca/encyclopedia/Photovoltaic_cell. [Accessed October 2022].

[5] Edis Osmanbasic, “Challenges of Making Solar Energy Economical”, *Engineering.com*, 2019. [Online]. Available: https://www.engineering.com/story/challenges-of-making-solar-energy-economical.

[6] Ahmad Faraj, Hassan Jaber, et al., “New Concept of Power Generation Using TEGs: Thermal Modeling, Parametric Analysis, and Case Study” *Entropy*, vol. 22, no. 503, Apr. 2020.

[7] Zhou, C., Lee, Y.K., Yu, Y. *et al.,* “Polycrystalline SnSe with a Thermoelectric Figure of Merit Greater Than the Single Crystal”. *Nat. Mater, v*ol. 20, Oct., pp.1378–1384, 2021.

[8] Hongchao Wang, Je-Hyeong Bahk, Chanyoung Kang et al., “Right Sizes of Nano and Microstructure for High Performance and Rigid Bulk Thermoelectrics”. *PNAS*, vol 30, July, pp. 10949-10954, 2014.

[9] J.-H. Bahk, "EECE/MECH7023 Graduate Course THERMOELECTRIC ENERGY CONVERSION: DEVICES AND CHARGE TRANSPORT," 2021.

[10] Kerry Taylor-Smith, “What Are Thermoelectric Ceramics?”, *AZO Cleantech*, 2019. [Online]. Available: https://www.azocleantech.com/article.aspx?ArticleID=987.[Accessed Sept. 2022].

[11] Margaret Wooldridge and Ralph H. Luebbers, “Heat Transfer,” *AccessScience*, McGraw Hill, 2020. [Online]. Available: https://www.accessscience.com/content/heat-transfer/311100. [Accessed August 2022].

[12] Kallista Wilson, “Heat Transfer Through Conduction; Examples in Everyday Life.” *Thermtest Instruments*, 2019. [Online]. Available: https://thermtest.com/heat-transfer-through-conduction-examples-in-everyday-life. [Accessed August 2022].

[13] “Heat Transfer by Convection,” *Byju’s*. [Online]. Available: https://byjus.com/physics/heat-transfer-convection. [Accessed August 2022].

[14] “Convective Heat Transfer Coefficients Table Chart”, *Engineers Edge.* [Online]. Available: https://www.engineersedge.com/heat_transfer/convective_heat_transfer_coefficients__13378.htm. [Accessed August 2022].

[15] Hadi Ali Madkhali and Ho-Sung Lee. “Modeling and Simulation of High-Performance Solar Thermoelectric Generator”, J Applied Mechanical Engineering, vol. 8, iss. 2, no. 320, 2019.

[16] Maria Theresa De Leon, Harold Chong, Michael Kraft. “Design and Modelling of SOI-Based Solar Thermoelectric Generators”. *Procedia Engineering*, vol 47, pp. 76-79, 2012.

[17] J.-H. Bahk and K. Yazawa, “Modeling and Optimization of Thermoelectric Modules for Radiant Heat Recovery,” *Novel Thermoelectric Materials and Device Design Concepts*, Skipidarov S., Nikitin M., Springer, 2019, pp. 297-324.

[18] “What is Emissivity and Why It Is Important?”, *National Physics Laboratory*, 2022. [Online]. Available: https://www.npl.co.uk/resources/q-a/why-is-emissivity-important. [Accessed September 2022].

[19] Gaurav A. Madhugiri and S. R. Karale. “High Solar Energy Concentration with a Fresnel Lens: A Review”. *International Journal of Modern Engineering Research*, vol.2, iss. 3, Jun., pp. 1381-1385, 2012.

[20] W.T. Xie, Y.J. Dai, R.Z. Wang, K. Sumathy. “Concentrated solar energy applications using Fresnel lenses: A review” *Renewable and Sustainable Energy Reviews*, vol. 15, Iss. 6, pp. 2588-2606, 2011.

[21] “Advantages of Fresnel Lens”, *Edmund Optics*, 2022. [Online]. Available: https://www.edmundoptics.com/knowledge-center/application-notes/optics/advantages-of-fresnel-lenses. [Accessed September 2022].

[22] Daniel Kraemer, Qing Jie, et al., "Concentrating solar thermoelectric generators with a peak efficiency of 7.4%". *Nature Energy*, vol. 1, no. 16153, Sept. 2016.

[23] Feng Cao, Daniel Kraemer, et al., “Enhanced Thermal Stability of W-Ni-Al2O3 Cermet-Based Spectrally Selective Solar Absorbers with Tungsten Infrared Reflectors”. *Adv. Energy Mater*., vol.5, no. 2, Sept. 2014.

[24] Ran He, Kornelius Nielsch, and Gabi Schierning. “Thermoelectric Devices: A Review of Devices, Architectures, and Contact Optimization”. *Adv. Mater. Technologies*, vol. 3, no. 1700256, 2017.

[25] Nanoelectronics Research Laboratory, Purdue University, “Tools: Create New Tool”, *nanoHUB*. [Online]. Available: https://nanohub.org/tools/create. [Accessed October 2022].

[26] “What is Version Control?”, *Atlassian Bitbucket*. [Online]. Available: https://www.atlassian.com/git/tutorials/what-is-version-control. [Accessed September 2022].

[27]. “How to Install Configure and Use SVN Subversion”, *Zapbuild*, 2010. [Online]. Available: https://www.zapbuild.com/bitsntricks/how-to-install-configure-and-use-svn-subversion. [Accessed September 2022].

[28] “15 Best Version Control Software (Source Code Management Tools)”, *Software Testing Help*, 2022. [Online]. Available: https://www.softwaretestinghelp.com/version-control-software. [Accessed September 2022].

[29] “Bismuth Telluride”, *American Elements*. [Online]. Available: https://www.americanelements.com/bismuth-telluride-1304-82-1 [Accessed October 2022].

[30] “Thermoelectric Materials 99.99% Bismuth Telluride Powder Price Bi2Te3 Powder”, Alibaba.com. [Online]. Available:

https://www.alibaba.com/product-detail/Bismuth-Telluride-Price-Bismuth-Telluride-Price_62307072189.html?spm=a2700.7724857.0.0.5dfd675f38yXMs&s=p [Accessed October 2022]

[31] David Feldman, Vignesh Ramasamy, et al., "U.S. Solar Photovoltaic System and Energy Storage Cost Benchmark: Q1 2020", NREL, Jan. 2021.

## References

Link to solarte Tool: https://nanohub.org/tools/solarte

Information on Nanohub's capabilities: https://nanohub.org/courses/tools/workshop2020

Example files to upload user's own thermoelectric properties data:
https://nanohub.org/resources/28715/supportingdocs

| | A | B | C | D | E | F |
|---|---|---|---|---|---|---|
| 1 | Temp (K) | Seebeck co | Thermal C | Electrical Conductivit | | *Please enter your data in the appropriate field and remove all entries in row 1 and 2 |
| 2 | | | | | | *and submit as such. Also please watch out for units. |
| 3 | 300 | 184.1411 | 1.07308 | 1174.056 | | |
| 4 | 320 | 190.6259 | 1.05558 | 1071.892 | | |
| 5 | 340 | 196.7105 | 1.04213 | 982.9119 | | |
| 6 | 360 | 202.4046 | 1.03339 | 904.8196 | | |
| 7 | 380 | 207.6972 | 1.0303 | 835.8385 | | |
| 8 | 400 | 212.5364 | 1.03407 | 774.7481 | | |
| 9 | 420 | 216.8335 | 1.04619 | 720.704 | | |
| 10 | 440 | 220.5338 | 1.06805 | 672.5737 | | |
| 11 | 460 | 223.5101 | 1.10138 | 629.8513 | | |
| 12 | 480 | 225.6515 | 1.14784 | 591.8677 | | |
| 13 | 500 | 226.8057 | 1.20918 | 558.2901 | | |
| 14 | 520 | 226.831 | 1.28695 | 528.7261 | | |
| 15 | 540 | 225.5815 | 1.38248 | 502.9295 | | |
| 16 | 560 | 222.9479 | 1.49681 | 480.4457 | | |
| 17 | 580 | 218.8126 | 1.63039 | 461.2658 | | |
| 18 | 600 | 213.1236 | 1.78318 | 445.1452 | | |
| 19 | 620 | 205.8741 | 1.95452 | 431.8705 | | |
| 20 | 640 | 197.1223 | 2.14295 | 421.3566 | | |
| 21 | 660 | 186.975 | 2.34672 | 413.3558 | | |
| 22 | 680 | 175.6029 | 2.56344 | 407.7415 | | |
| 23 | 700 | 163.2299 | 2.79034 | 404.3808 | | |
| 24 | 720 | 150.1017 | 3.02467 | 403.1003 | | |

*Figure 52: Example User Input Data File*